Chapter 6

Ice-Phase Precipitation

I. GULTEPE

Cloud Physics and Severe Weather Research Section, Environment Canada, Toronto, Ontario, Canada

A. J. HEYMSFIELD

National Center for Atmospheric Research, Boulder, Colorado

P. R. FIELD

*Met Office, Exeter, and School of Earth and Environment, Institute for Climate and Atmospheric Science,
University of Leeds, Leeds, United Kingdom*

D. AXISA

National Center for Atmospheric Research, Boulder, Colorado

ABSTRACT

Ice-phase precipitation occurs at Earth's surface and may include various types of pristine crystals, rimed crystals, freezing droplets, secondary crystals, aggregates, graupel, hail, or combinations of any of these. Formation of ice-phase precipitation is directly related to environmental and cloud meteorological parameters that include available moisture, temperature, and three-dimensional wind speed and turbulence, as well as processes related to nucleation, cooling rate, and microphysics. Cloud microphysical parameters in the numerical models are resolved based on various processes such as nucleation, mixing, collision and coalescence, accretion, riming, secondary ice particle generation, turbulence, and cooling processes. These processes are usually parameterized based on assumed particle size distributions and ice crystal microphysical parameters such as mass, size, and number and mass density. Microphysical algorithms in the numerical models are developed based on their need for applications. Observations of ice-phase precipitation are performed using in situ and remote sensing platforms, including radars and satellite-based systems. Because of the low density of snow particles with small ice water content, their measurements and predictions at the surface can include large uncertainties. Wind and turbulence affecting collection efficiency of the sensors, calibration issues, and sensitivity of ground-based in situ observations of snow are important challenges to assessing the snow precipitation. This chapter's goals are to provide an overview for accurately measuring and predicting ice-phase precipitation. The processes within and below cloud that affect falling snow, as well as the known sources of error that affect understanding and prediction of these processes, are discussed.

1. Introduction

The major components of snow precipitation are related to processes occurring in and below clouds such as nucleation, depositional growth, collision–coalescence, accretion, aggregation, sublimation, secondary ice generation, and freezing. Thermodynamical and dynamical conditions affect the rate at which these processes occur,

and hence both the intensity and amount of snow within the cloud and at the surface. Thus, for accurate prediction of snow, knowledge of not only microphysical processes within the cloud but also conditions related to the ambient dynamics and thermodynamics of the system are required.

The goals of this chapter are to provide an overview of what is important for accurately observing and predicting ice-phase precipitation, the processes within and below cloud that affect falling snow, the known sources

of error that affect the understanding and prediction of these processes, and the steps needed to improve snow estimates. Prediction of solid precipitation based on various model types that include cloud, numerical weather prediction (NWP), and climate models can include issues related to scale and downscaling issues, microphysical schemes, parameterizations, data assimilation, and boundary conditions. Thus, specific sections on methods used to measure snow, its prediction, and their inherent limitations and uncertainties, are presented. The current status of the prediction of snow precipitation at various scales and the effects of snow on weather, climate, and society are included, as well as recommendations for future work.

2. Description of the ice-phase precipitation and microphysics

Solid precipitation, including both single and complex snow crystals, is very important in precipitation process. Based on the American Meteorological Society (AMS) Glossary of Meteorology (American Meteorological Society 2016a), snow is defined as precipitation composed of white and/or translucent ice crystals, chiefly in complex branched hexagonal form and often aggregated into snowflakes that fall onto Earth's surface. Ice crystal formation can occur because of various nucleation processes. These nucleation processes (see Kanji et al. 2017, chapter 1) are usually defined as 1) homogeneous nucleation and 2) heterogeneous nucleation (Gultepe et al. 2016). Depending on ice nuclei chemical and physical properties, ice crystals as a function of dynamical and thermodynamic conditions can have various habit and particle size distributions. After nucleation, ice crystals of different habits such as "pristine" needles, plates, columns, dendrites, and stellar crystals grow according to the relative humidity RH with respect to water (RH_w) and temperature T. However, observed particles commonly have many nonpristine shapes. Lawson et al. (2006) reported that irregularly shaped ice crystals at T between $-30°$ and $-40°C$ were observed in an Antarctic site during all types of falling ice crystal precipitation and in blowing snow, which was prevalent when the wind speed was $4 \, m \, s^{-1}$. Irregular ice crystals in blowing snow were observed to generally have more rounded edges than irregular shapes in precipitation. These were consistent with diamond dust, and falling ice fog/light snow particles were observed in the Arctic region (Gultepe et al. 2015). In addition to diffusional growth, collision and aggregation because of turbulence, eddies, and different fall velocities, as well as collection and freezing of supercooled droplets (riming), can affect precipitation characteristics. Under mixed-phase and dynamically active conditions, ice particles can develop into graupel and hail at higher altitudes in the cloud. The terminal velocity V_t of ice crystals is typically between 0.1 and $3 \, m \, s^{-1}$, and the vertical air velocity w_a plays an important role in the particle growth and ultimately snow precipitation intensity (Heymsfield et al. 2007; Gultepe et al. 1995; Gultepe and Starr 1995). Snow crystal densities (mass divided by spherical volume based on particle maximum size) usually vary from 0.05 to $0.20 \, g \, cm^{-3}$, which is size dependent because mass is related to crystal size (Cotton et al. 2013). After precipitating ice particles fall below cloud base, they experience evaporation, turbulence, collision and mixing processes before reaching the ground. A large fraction of Earth's rain originates as snow that subsequently melts before reaching the ground (Field and Heymsfield 2015).

The increasing size of ice particles depends on both the dynamics of the system (e.g., turbulence, eddies, updrafts) and the thermodynamics of the environment (e.g., cooling rates and ice nuclei) (Gultepe et al. 2000). Further growth of ice particles by riming and aggregation is a function of the droplet spectra and ice crystal morphology, which affects the ice particle–droplet or ice crystal–crystal collision efficiency (defined as the ratio of collisions to all particles) and the aggregation efficiency (defined as ratio of merging ice crystals to all collisions (Pflaum and Pruppacher 1979). Mixed-phase conditions leading to snow can also be affected by ice crystals at the expense of droplets, which is a result of the vapor pressure difference between droplet and ice particle surfaces (Bergeron 1935) and through the riming process.

Ice microphysical properties can be related to ice nuclei (IN) physical properties and their chemical composition (Shantz et al. 2014). The IN number concentration plays an important role for ice crystal growth that is a function of both T and available moisture. Previous studies suggest ice crystal number concentrations N_i within a cloud may well exceed those of ice nucleating particles (INPs) based on observations and parameterizations (e.g., Fletcher 1962; Hobbs 1975). These studies suggested that ice multiplication may have occurred when the measured N_i is much larger than predicted by the Fletcher (1962) study for a given temperature. Ice multiplication here is defined as increasing N_i based on microphysical, dynamical, and thermodynamic processes beyond their natural formation and its details are given in section 8b(2). Mossop (1978) found that secondary ice production [SIP; see Field et al. (2017, chapter 7) for more details] occurs at certain temperatures and for certain sizes of both the ambient droplets and ice crystals. SIP process usually results in the rapid

glaciation of a cloud (Lawson et al. 2015), leading to increasing precipitation.

The aggregation (combination of two or more crystals) of ice crystals plays an important role for snow precipitation intensity because of increasing mass (Lo and Passarelli 1982). It depends on the relative terminal velocity of the aggregated components, their sticking efficiency (defined as possibility of joining together of particles after the collision; Phillips et al. 2015), wind shear, turbulence, T, RH, and electrical charge (Saunders and Wahab 1975). The density and shape of the ice particles, which influences the precipitation amount (PA) and snow depth, are strong functions of the environmental conditions that affect the ice nucleation processes, radiative heating, cooling, and turbulence. More specifically, the rate of collision depends upon the relative fall speeds and sizes (Stokes number), cross-sectional areas and, possibly, electrical charge. The nature of crystal attachment in the atmosphere is not well understood, but potentially important factors for controlling the sticking efficiency are related to the shape of ice crystals (e.g., mechanical interlocking of dendrites), surface properties (also its morphology; Phillips et al. 2015), and atmospheric thermodynamical properties (T, RH) that promote rapid sintering between crystals and electrical charges. Laboratory investigations into aggregation of snow particles were studied by Hosler and Hallgren (1960) and Connolly et al. (2012). On the other hand, a few aircraft-based attempts at quantifying sticking efficiency were also performed by Passarelli (1978), Mitchell (1988), Field and Heymsfield (2003), and Field et al. (2006). These studies typically show that 1 collision in 10 results in a sticking event if a simple gravitational collection kernel is used to estimate the rate at which collisions occur.

Below the cloud base, subsaturation of air with respect to ice can result in sublimation of the ice and snow particles. When air becomes slightly less saturated with respect to water below the cloud base, then ice particle growth during fall can still occur (Field et al. 2007; McFarquhar et al. 2007). This growth can affect the snow water equivalent (SWE, defined as the ratio of melted snow amount to snow depth) of the precipitation on the ground and needs to be studied because aggregation during sublimation is usually neglected in modeling simulations.

In clouds with strong updrafts, riming of snow crystals, snowflakes, and graupel particles may continue where hail can develop (Knight et al. 1982). Hail, by definition, has a diameter of 5 mm or more (Lin et al. 1983). The AMS Glossary of Meteorology (American Meteorological Society 2016b) defines graupel as heavily rimed snow particles that are distinguished by conical, hexagonal and lump forms, whereas hail is defined as balls or irregular lumps of ice (American Meteorological Society 2016b,c). The bulk density of these particles is related to the ice particle surface, environmental T and RH, and the liquid water content. The bulk microphysics algorithms in cloud or forecast models, with varying degrees of complexity (one- or two-moment schemes), can be used to predict parameters related to cloud ice crystals, precipitating snow particles, graupel, and hail (Morrison and Milbrandt 2011). Microphysical processes for converting between hydrometeor types are not well constrained. Figure 6-1 (from Tomita 2008) shows the major components of a six-class microphysical scheme used in simulations of cloud systems. The major components of this scheme are vapor, cloud water, cloud ice, rain, and snow, as well as graupel. Interactions among these components are shown with various transformations. The rate at which these transformations occur is highly dependent on assumptions used in the scheme, including the spectral form of size distributions and particle fall velocities, shapes, and collection efficiencies. A major uncertainty for snow formation is to better understand how the autoconversion process is parameterized between various phases of snow and ice crystals, and develop physically based particle growth models without preassumed empirical relationships for microphysical parameters.

In this chapter, snow measurements and microphysics are provided in section 3. The cloud microphysics are given in section 4. Then snow prediction issues based on various numerical models are summarized. Section 6 focuses on precipitation efficiency calculation and related issues. Snow precipitation's effects on weather, climate, and society are analyzed in section 7. Sections 8 and 9 summarize the challenges to understanding snow precipitation and recommendations for future work, respectively.

3. Snow measurements and microphysics

Measurements of snowfall are made using weighing gauges and optical sensors (Table 6-1) (Gultepe et al. 2016). Weighing gauges (e.g., Geonor or Pluvio models) melt the fallen snow using chemicals and weigh the water afterward. Optical probes (e.g., disdrometers) provide either snow crystal size and shape distribution, or bulk parameters such as precipitation rate (PR) or PA, based on the measured fall velocities. Optical-probe-based visibility (Vis) measurements [present weather detector (PWD) or SWS200 present weather
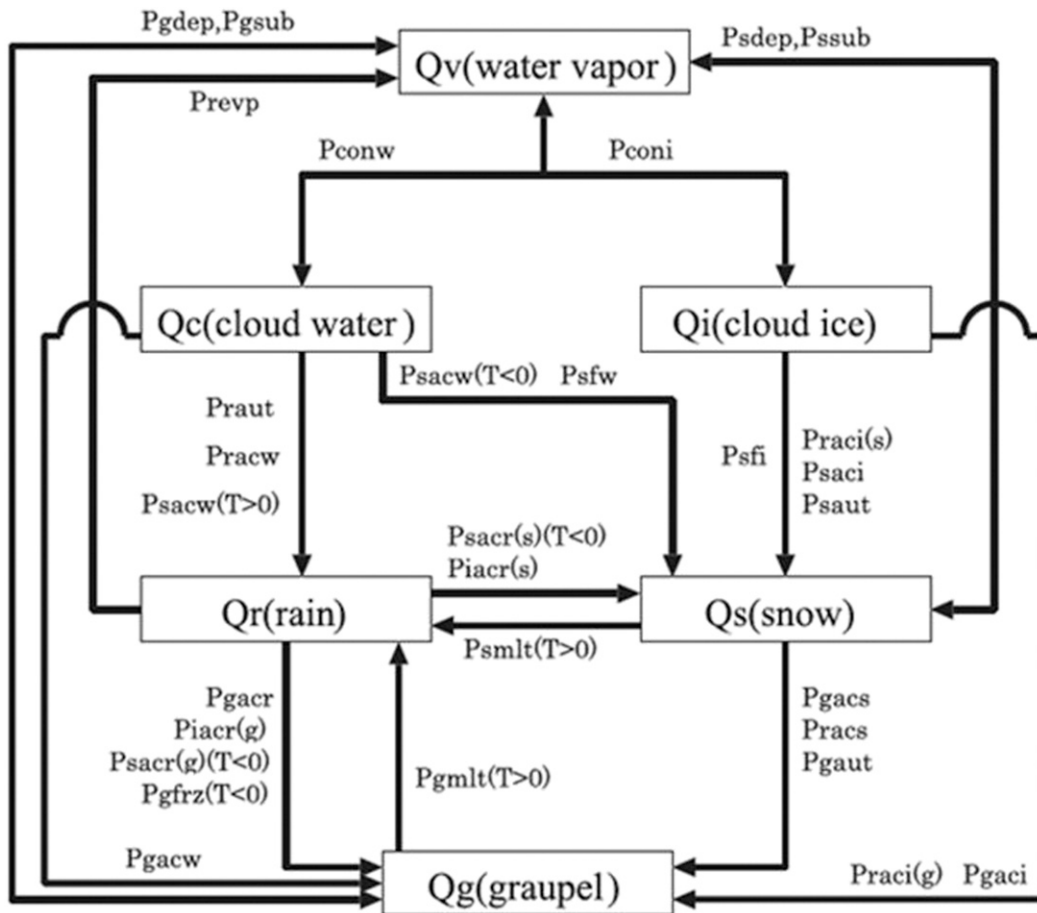
FIG. 6-1. Conversion diagram for the six-class one-moment microphysical scheme applicable to global cloud-resolving simulations. It shows interactions among main precipitation and cloud physical and thermodynamic parameters, and processes among various parameters, e.g., autoconversion due to collision–coalescence, aggregation, and ice multiplication (adapted from Tomita 2008).

sensors; Table 6-1] also provide PA and PR, and bulk precipitation type. SWE is usually obtained by a ratio of measuring melted amount of snow (mm) measured by weighing gauges to snow depth (mm) measured by snow rulers or snow depth sensors such as SR50, and it can change from a few percent up to more than 50% depending on snow particle morphology.

By definition, snow precipitation can include various particle shapes and types, and the SWE ratio is usually assumed to be 10% by forecasters. The U.S. National Weather Service (NWS) previously used a SWE conversion table as a function of T (Table 6-2; NWS 1996; Dubé 2003). It is unlikely that this table will be used operationally because of the variability in SWE as a function of temperature and particle type. The amount of water within the snow can play an important role for the hydrological cycle, environmental processes, and also for transportation and aviation. The surface

skin temperatures can also affect precipitation type, for example, freezing drizzle, rain, or snow. Snow types can also be divided into various subgroups such as ice or snow pellets, wet snow and ice crystals (Dubé 2003). Figure 6-2 shows various snow particle types collected during the Fog and Remote Sensing and Modeling (FRAM) and Satellite Application for Arctic Weather and Search and Rescue (SAR) Operations (SAAWSO) projects (Gultepe et al. 2015; Rabin et al. 2016).

Ice pellets (or sleet) are usually defined as frozen raindrops (Dubé 2003). Based on their density, ice pellets can be classified into the heavy snow category. He stated that in the presence of a deep warm layer ($T > 3$°C) above a layer with freezing temperatures ($T < -5$°C), drops can form from melting of the snow crystals in the warm layer, then fall into the cold air layer, leading to their freezing and formation of sleet.

TABLE 6-1. Shows precipitation- and visibility-measuring sensors (Gultepe et al. 2016). Precipitation type (PT), precipitation rate (PR), particle spectra (PS) and amount (PA), visibility (Vis), fall velocity (V_f), and diameter (D).

Precipitation and Vis sensors	Manufacturing company	Measurements	Threshold PR, PA, Vis
GCIP	DMT	PS, shape	$0.01\,mm\,h^{-1}$
PWD22	Vaisala	PT, PR, PA, Vis	$0.01\,mm\,min^{-1}$ ($0.05\,mm\,h^{-1}$), 0.01 mm and 10%, $>-40°C$, 10 m (10%)
FD12P	Vaisala	PT, PR, PA, Vis	$0.02\,mm\,min^{-1}$ ($0.05\,mm\,h^{-1}$), 0.01 mm and 10%, $>-40°C$, 10 m (10%)
SWS200	Biral	PT, PR, PA, Vis	$0.0015\,mm\,h^{-1}$, 0.001 mm, 10 m, 5%, $>-40°C$
OSI-430	Optical Scientific	PT, PR, PA, Vis	$0.01\,mm\,h^{-1}$, 0.001 mm, 0.001 km, $>-40°C$
Sentry	Envirotech	Vis	10%, 30 m, $>-40°C$
LPM	Thiessen	PT, PS, PR, PA, V_f, Vis	$0.005\,mm\,h^{-1}$, 0.005 mm, $>-40°C$, D [0.16–>8 mm], V_f [0.2–20 m s^{-1}], up to 30%
Geonor-200	Geonor	PR, PA	$0.05\,mm\,h^{-1}$, 0.05–0.1 mm, $>-40°C$
TPS	Total Precipitation Sensor	PR, PA	$0.01\,mm\,h^{-1}$, 0.1 mm
Pluvio	OTT	PR, PA	$12\,mm\,h^{-1}$ or $0.20\,mm\,min^{-1}$, 0.10 mm, $>-40°C$

Snow grains (frozen water droplets) are also included in this category. Details on the basic precipitation processes for modeling applications have been described in many studies, including Lin et al. (1983), Tomita (2008), Ferrier (1994), Ferrier et al. (1995), Milbrandt and Yau (2005), and Morrison et al. (2005). In the following sections, snow measurements and its microphysics are provided.

a. Weighing gauge measurements and uncertainties

Weighing precipitation gauges are affected by the environmental conditions, especially by the horizontal wind speeds and turbulence. Under relatively calm wind conditions (horizontal wind speed $U_h < 5\,m\,s^{-1}$), Geonor and Pluvio (Fig. 6-3a) measurements may not need wind corrections for heavy rain but their sensitivity for light snow (LSN) and light rain (LRN), including drizzle, can be an important issue (Gultepe et al. 2016; Leeper et al. 2015). Usually, a double-fenced weighing gauge (Fig. 6-3b) is used for reference snow measurements. Figure 6-3c shows the entire project area called PanAm University of Ontario Meteorological Supersite (PUMS) nearby Oshawa, Ontario, Canada. Both Pluvio and Geonor measurements with an alter shield in a bush environment or within a double-fenced international reference (DFIR) system are usually accepted as reference for precipitation measurements. Geonor observations of snow PR have an uncertainty of $0.1\,mm\,h^{-1}$ based on the factory specification, but this sensitivity can be up to $0.5\,mm\,h^{-1}$ with turbulence and stronger wind conditions (Gultepe et al. 2016). The Geonor weighing gauge utilizes a technology based on three vibrating wires to measure the weight of melted snow

in a bucket to distribute the snow mass equally. These measurements are then converted to precipitation amount over 5–10-min intervals. Another sensor for the snow measurements can be used is the total precipitation sensor (TPS; Rasmussen et al. 2012). Although its measurements can be reliable for stable atmospheric conditions, because of high winds and strong turbulence, TPS measurements can include large uncertainties (Boudala et al. 2014). For winds greater than $8\,m\,s^{-1}$, a $1\,mm\,h^{-1}$ threshold value is needed to obtain accurate PR for both the TPS and Geonor 5-min averaged measurements (Rasmussen et al. 2012).

b. Optical probes

As stated above, snow measurements at the surface can be measured by optical probes based on the extinction coefficient and spectral snow crystal characteristics. The Ground Cloud Imaging Probe (GCIP; Fig. 6-4a) was developed by Environment Canada (Fig. 6-4a). It is based on the Droplet Measurement Technologies (DMT) Cloud Imaging Probe (CIP), which

TABLE 6-2. Conversion of snow amount to equivalent water (NWS 1996).

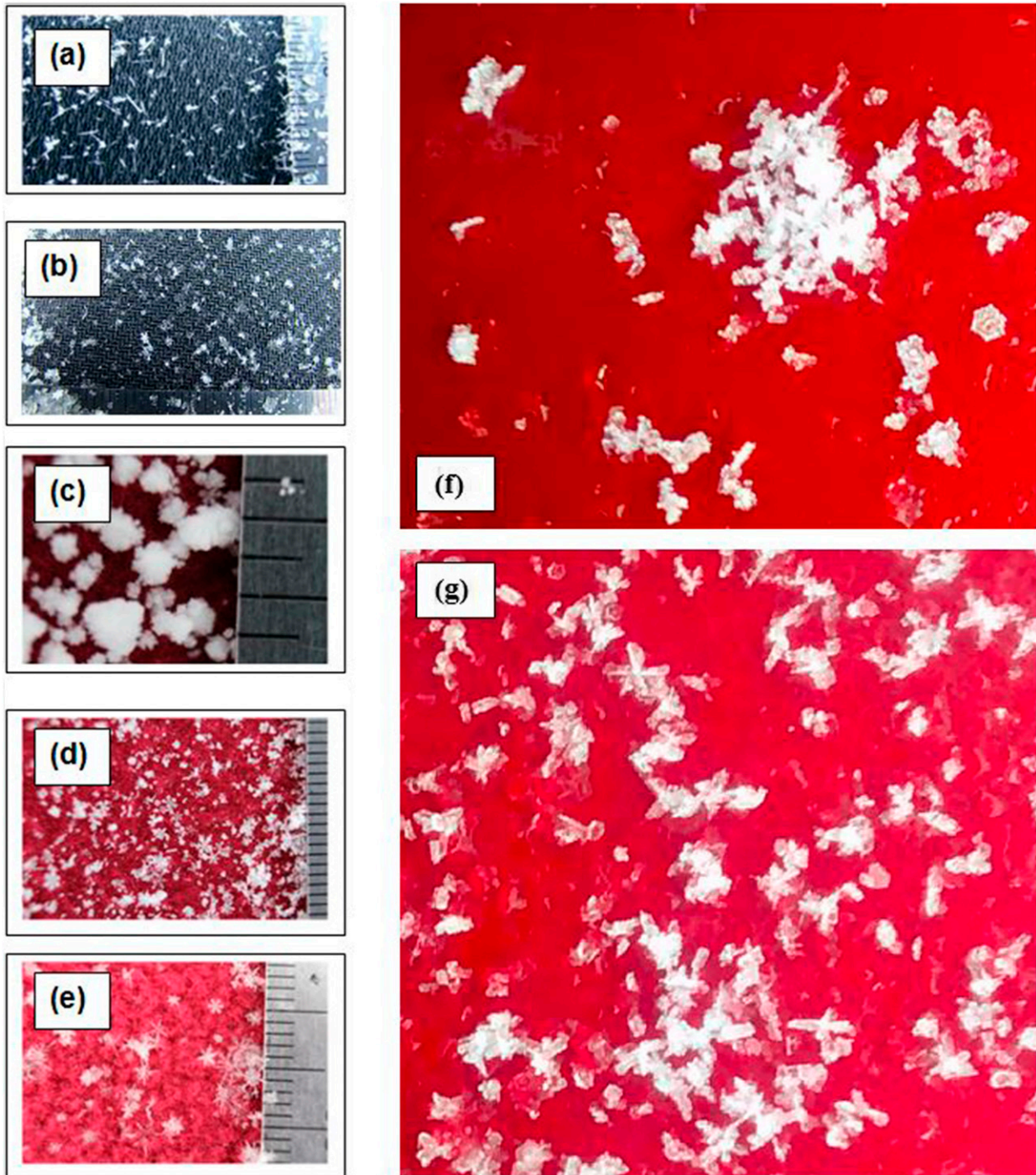| Surface temperature (°C)	Snow/water ratio
−2.22 to −1.11	10:1
−6.67 to −2.78	15:1
−9.44 to −7.22	20:1
−12.22 to −10.00	30:1
−17.78 to −12.78	40:1
−28.89 to −18.33	50;1
−40.00 to −29.44	100:1

FIG. 6-2. Snow particles collected during FRAM and SAAWSO projects that took place during 2010–15 winters. (a) Secondary ice crystal generated by splintering mechanism over Whistler Mountain, (b) small wet ice crystals, (c) graupel, (d) rimed single ice crystals, (e) light snow crystals, (f) rimed and aggregated snow crystals, and (g) high density ice pellets. Scales between 2 lines in (a)–(e) is 1 mm; (f) and (g) have a snow crystal maximum size of 3 and 1 mm, respectively.

nominally images particles between $D_{\min} = 7.5 - D_{\max} = 930\,\mu\mathrm{m}$ where D is diameter (Gultepe 2008; Gultepe et al. 2015). The LSN precipitation rate (PR$_{\mathrm{LSN}}$) is defined as PR $< 0.5 - 1.0\,\mathrm{mm\,h}^{-1}$ and is usually not measured

accurately by weighing gauges such as Geonor or Pluvio instruments (Fig. 6-4b) because of their PR detection threshold of $0.1 - 0.5\,\mathrm{mm\,h}^{-1}$, and when the wind speeds are high. The goal of the GCIP development was to
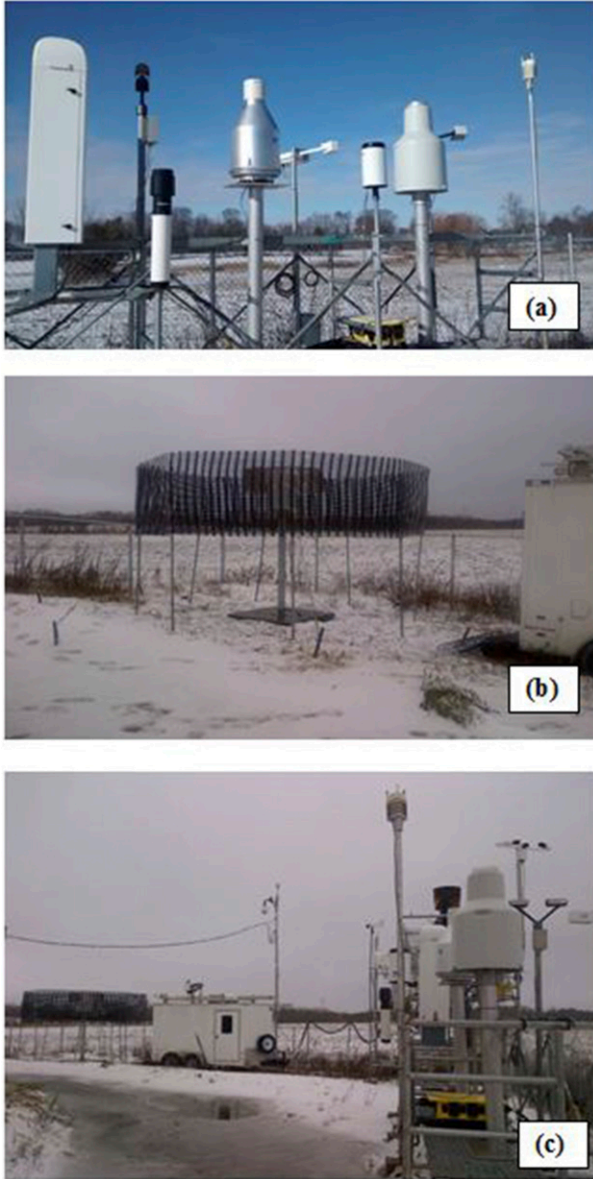
FIG. 6-3. Various precipitation sensors at the PUMS site near Toronto, Ontario, Canada. (a) The Geonor, Pluvio, Yonge tipping-bucket, capacitor sensor, and WXT52. (b) A double-fenced reference system with Pluvio sensor (scaled down to 1.5 times), similar to the DFIR reference platform. (c) Entire project area (PUMS site) in Oshawa.

detect and measure light snow, light rain, and ice fog microphysical parameters that can be used to support the measurements of disdrometers and fog devices. The GCIP, in combination with a laser precipitation monitor (LPM; Fig. 6-4c), covers the hydrometeor radius range from 7.5 μm up to centimeter size ranges, including LSN particles (e.g., less than 500 μm). In addition to GCIP, the fog-measuring device (FMD; also called FM100; Fig. 6-4d) has been used during the FRAM and

SAAWSO projects to study ice and freezing fog conditions (Gultepe et al. 2014b, 2015). A two-dimensional video disdrometer (2DVD) has also been used for snow spectral measurements at 0.2-mm resolution (Löhnert et al. 2011; Brandes et al. 2007). The DMT Meteorological Particle Spectrometer (MPS) precipitation sensor (50 μm–6.4 mm), adapted from the aircraft 2D-P probe, is used for measuring the size and fall velocity of snow crystals at the surface, providing particle shape and size spectra. The new sensor called Multi-Angle Snowflake Camera (MASC), which was developed for snow crystal microphysical property measurements, takes stereographic photographs of hydrometeors at 9–37-μm resolution (Garrett et al. 2012). The camera is triggered by a vertically stacked bank of sensitive infrared (IR) motion sensors designed to filter out slow variations in the ambient light. The MASC uses multiple cameras at three angles to measure falling snow spectral properties, its habit, and fall speed that occur over sizes ranging from 100 μm up to 10 cm. Similar to the MASC, the Ice Crystal Imaging Probe (ICIP) based on a single camera system is developed (Kuhn and Gultepe 2016; Gultepe et al. 2014a,b) for light snow and ice fog measurements that can measure ice crystals from a few micrometers up to 500 μm.

The PR for snowfall using GCIP with 63 bins between maximum and minimum crystal sizes (D_{min} and D_{max}, respectively) can be obtained as

$$\text{PR}_{\text{GCIP}}(\text{mm h}^{-1}) = A_c \sum_{\text{Dmin}}^{\text{Dmax}} V_i(D)\rho_s(D)N_i(D)V_t(D),$$

(6-1)

where $V_i(D)$ (cm^3) is the snow crystal volume for a particle of diameter D based on maximum dimension, ρ_s is the snow crystal effective density, and A_c is the conversion factor from seconds to hours. To compute PR_{GCIP}, empirical relationships between mass and size are used, and terminal velocity V_t is obtained from the known particle spectra with bins of $\Delta D = 15 \mu$m. In Eq. (6-1), ice crystal mass is given as $m(D) = V_i(D)\rho_s(D)$, which is a function of particle shape. Therefore, accurate measurements of PR from spectral optical sensors require better snow crystal shape assessment and accurate empirical relationships between V_t, mass, and size parameters. In reality, V_t depends primarily on the mass-to-projected area ratio (m/A), and hence empirical relationships for V_t (e.g., $V_t = aD^b$) implicitly combine both mass– and area–size relations in numerical models. The V_t schemes like Heymsfield and Westbrook (2010) avoid potential inconsistencies by using explicit m–D and A–D expressions like those presented in Erfani and
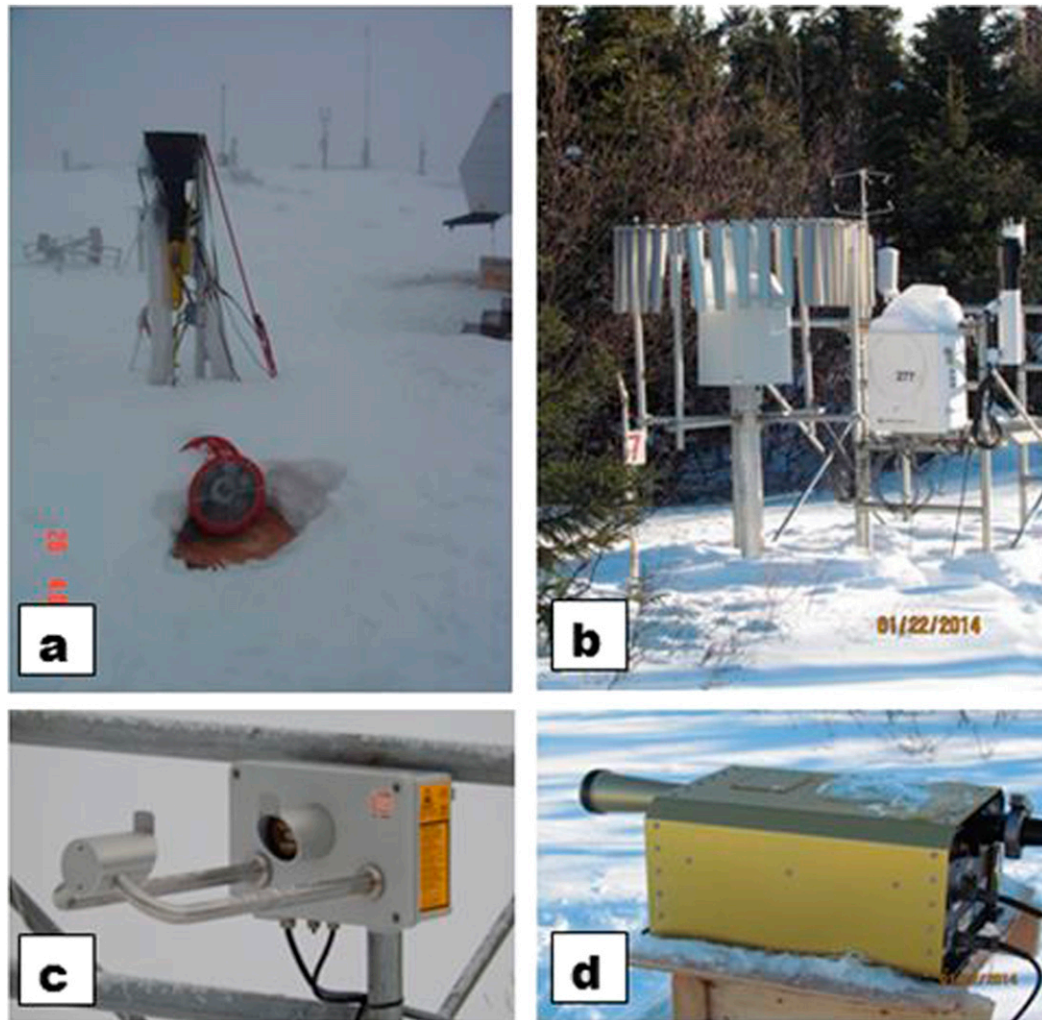
FIG. 6-4. (a) GCIP instrument for snow spectral measurements at sizes less than about 1 mm. (b) Pluvio instrument with a single-alter shield at 3-m height with a Metek Inc. 3D ultrasonic anemometer. (c) LPM for snow spectral measurements. (d) DMT Inc. FMD (FM100) to measure fog particle spectra between 1 and 50 μm over 16 channels.

Mitchell (2016) that can be made to be consistent throughout a model.

Cloud particle measurements are required to range from sizes less than a few tens of micrometers to centimeters in diameter to better verify precipitation processes in operational applications and numerical model simulations. The best way to operationally measure cloud/fog bulk particle characteristics and light snow precipitation hydrometeors is to use optical present weather sensors (OPWS; Gultepe et al. 2009, 2014a,b) such as the PWD52 (from Vaisala Inc.) and SWS (from Metek Inc.). These sensors use either a constant value of SWE as 10% or internal algorithms based on particle type to obtain the melted snow amount. This technique can lead to inaccuracies in snow measurements (Gultepe et al. 2016). The OPWS sensors can work accurately for LSN conditions compared to heavy snow conditions because the constant SWE can be modified with respect to falling ice crystals type. The SWS uses both forward and backscattering techniques for precipitation and visibility measurements.

c. Disdrometer measurements

Disdrometers such as the Thies LPM and OTT disdrometers (Gultepe et al. 2014b; Jaffrain and Berne 2011), with special bin intervals, can be used for snow precipitation and fall velocity measurements. The LPM sensor (Thies Clima 2007), shown in Fig. 6-4, uses a laser source (laser diode and optics) that produces a parallel near-IR light beam (0.780 μm with 0.5-mW optical power, 40–47 cm^2 measuring an area with $x = 228$ mm, $y = 20$ mm,

and $z = 75$ mm). When a precipitation particle falls through the light beam (measuring 45.6 cm^2 area), the signal received is reduced. The diameter of the particle is calculated from the amplitude of the reduction, and the fall speed from the duration of the reduced signal. Output parameters include the intensity, quantity, type of precipitation (drizzle, rain, snow, and hail as well as mixed precipitation), and the particle size distribution. Data are sorted into 22 different diameter bins from 0.125 mm up to >8.0 mm and into 20 fall speed bins from 0 up to >10 m s^{-1}. Traditional optical sensors (e.g., disdrometers) are not capable of measuring LSN PR because of their weak optical response for sizes $<200\,\mu$m (Tapiador et al. 2012; Yang et al. 1999; Brandes et al. 2007).

d. Correction of snow measurements from weighing gauges

Instrument technical issues related to the detection of small particle size and mass, and to the conditions such as low temperature, wind, and turbulence can affect weighing gauges' measurement capabilities (WMO/CIMO 1991; Gultepe et al. 2016). Zhang et al. (2004) proposed correction methods as a function of temperature T (°C) and horizontal wind U_h (m s^{-1}) for snow, rain, and mixed-type precipitation measurements. They provided the catch ratio [CR (%)] defined as the ratio of amount of precipitation received by the sensor to this of a reference sensor for snow, mixed, and rain, respectively, as

$$\mathrm{CR}_S = 103.10 - 8.67 U_h + 0.30 T_{\max}, \tag{6-2}$$

$$\mathrm{CR}_M = 96.99 - 4.46 U_h + 0.88 T_{\max} + 0.22 T_{\min}, \tag{6-3}$$

and

$$\mathrm{CR}_R = 100.0 - 4.77 U_h^{0.56}. \tag{6-4}$$

The terms $T_{\max}$ and $T_{\min}$ are maximum and minimum daily temperatures, respectively. Zhang et al. (2015) subsequently proposed CR relationships for the Geonor instrument measuring snow as a function of U_h by Smith (2009) and MacDonald and Pomeroy (2007), respectively, as

$$\mathrm{CR}_{GD} = \frac{P_{\mathrm{Geonor}}}{P_{\mathrm{DFIR}}} = \exp(-0.2 U_h), \quad \text{and} \tag{6-5}$$

$$\mathrm{CR}_{GN} = \frac{P_{\mathrm{Geonor}}}{P_{\mathrm{Nipher}}} = 1.10 \exp(-0.09 U_h). \tag{6-6}$$

The above equations were derived using a DFIR system with a Geonor inside and a Geonor instrument with Nipher shield (Metcalfe et al. 1997). The subscripts DFIR and Nipher represent snow precipitation measured by the DFIR setup and by the corrected Nipher and Chinese standard precipitation gauge setup, respectively. When Geonor is not used with a DFIR platform, the above equations can be used for snow measurement corrections. Operational stations usually provide total snowfall amount over the large range of hours; therefore, they are subject to wind-induced errors that can be more than 50% (Yang et al. 1999; Sevruk et al. 2009). Other corrections for snow measurements from weighing gauges are because of light snow particles, wetting, and evaporation; more information on these corrections can be found in Gultepe et al. (2016) and Yang et al. (2005).

4. Cloud microphysics and its relation to snow precipitation

Cloud microphysical processes are important for the formation of snow precipitation at the surface and these together with in situ measurements are discussed below.

a. In-cloud microphysics measurements

In-cloud microphysical measurements have been performed for many years (Knollenberg 1969, 1972; Heymsfield et al. 2011, 2007; McFarquhar et al. 2007; Kelly and Vali 1991; Lawson et al. 2015), and they are important for understanding precipitation processes. The production of ice crystals in clouds has significant implications on snow precipitation efficiency (Gultepe et al. 2016). Snow precipitation intensity can change depending on whether clouds are convective or stratiform. Aircraft in situ observations of ice and snow particles are used to develop microphysical parameterizations for snow particles, ice crystals, droplets, and mixed-phase precipitation. Precipitation-sized particles have been measured by the Stratton Park Engineering Company (SPEC) 2D stereo probe (2D-S) and Cloud Particle Imager (CPI; 10-μm resolution) (Lawson et al. 2015), the DMT CIP (25–1550 μm), 2D cloud probe (2D-C; 25–1600 μm), 2D precipitation probe (2D-P; 100–6400 μm), SPEC High-Volume Precipitation Spectrometer (HVPS), and DMT 2D precipitation imaging probe (2D-PIP; 100–6200 μm) precipitation probes (DMT Inc. 2004; Sukovich et al. 2009). The HVPS (with spectra size range of 0.2 mm–4.2 cm) manufactured by SPEC Inc. mounted on aircraft has been used for measuring large snow crystals (Lawson et al. 1993a,b, 1998). The HVPS has about 30 times larger sample volume and 7 times larger viewing area compared to the PMS 2D-P probe. Snow precipitation particle sizes are usually larger than 200 μm, which is a lower threshold for ice particles to acquire sufficient size to fall from a cloud and can

reach diameters up to a few centimeters in size. Detailed studies of ice microphysical measurements from convective systems have been performed by Heymsfield and Willis (2014), Heymsfield (2003), Field et al. (2007), McFarquhar et al. (2000), Lawson et al. (2015), and others.

Measurements from weather systems with high liquid and ice water content (LWC and IWC) (e.g., convective systems) can be difficult because of large updrafts and icing of the sensors. Figure 6-5 shows precipitating and cloud particles observed during the Ice in Clouds Experiment–Tropical (ICE-T) project at various temperatures (Lawson et al. 2015). Their work suggested that decreasing T results in different snow crystal types, and increasing temperature results in more graupel and melted snow particles. In the rapid glaciation region of convective cloud systems, more spherical droplets and frozen particles with splintering ice crystals are observed. Warmer temperatures with faster cooling processes likely resulted in rapid glaciation and secondary ice production processes (Lawson et al. 2015). The initiation and rapid development of ice in tropical and extratropical maritime clouds with cloud tops warmer than $-10°C$ has been a research focus for many years (Mossop et al. 1970; Hobbs and Rangno 1990). Lawson et al. (2015) suggested that in order for supercooled drops to freeze, updraft velocities in the range from about 7 to $10 \, m \, s^{-1}$ are required, and small velocity variations with time do not greatly affect the processes. If updraft velocities are less than about $5 \, m \, s^{-1}$, the largest drops fall out of the updraft and are not frozen, resulting in slower ice development. The Fast Forward Scattering Spectrometer Probe (FFSSP), CPI, and 2D-S in Fig. 6-5 (Lawson et al. 2015) show that large droplets can be quickly depleted during the rapid glaciation process when millimeter-size frozen drops and graupel particles are present (row 1–3 in Fig. 6-5). The tail of the drop size distribution (DSD) decreased from $3 \, \mu m$ in the first ice region ($-8°$ to $-11°C$, panels in row 1 of Fig. 6-5) to about $300 \, \mu m$ in the rapid glaciation region ($-12°$ to $-20°C$, panels in rows 2–3 of Fig. 6-5). The left panel in row 3 of Fig. 6-5 shows increasing cloud-top height, and the middle panel shows the particle size distribution (PSD) obtained from the FFSSP, 2D-S, and HVPS. The right panel shows the glaciated particle images and representative spectra for liquid and ice particles. Examples of particle images representing droplets and ice crystals from 2D-S probe are shown in the left panel of row 4. The droplets and ice particle spectra and their representative LWC, IWC, and reflectivity factor Z values within the glaciation region ($-12°$ to $-20°C$) are shown in the right panel of Fig. 6-5. The difference between small ice particles and large supercooled drops fall velocities in a turbulent environment can result in a riming process

whereby droplets freeze on contact with the small ice crystals (Heymsfield and Willis 2014). This in turn produces secondary ice particles such as the rime-splintering (Ovtchinnikov and Kogan 2000; Hallet and Mossop 1974) or ice-to-ice collision processes (Vardiman 1978), resulting in more frozen drops and ice crystals, and forcing rapid glaciation. Examples of droplets, frozen droplets, and graupel are shown in the left panel of row 4. The liquid and ice PSD and averaged LWC and IWC in the rapid glaciation region ($-12°$ to $-20°C$) are shown in right panel in row 4.

Arctic cloud systems usually form during stable atmospheric conditions and include various ice crystals types that transform to snow; their mass density is relatively small because of cold temperatures. Zhang et al. (2014) used U.S. Department of Energy (DOE) North Slope Alaska (NSA) ground site and aircraft observations to study N_i profiles derived from 2D-C probe measurements and from retrievals of W- and X-band airborne radars and ground-based cloud radars. They also compared riming conditions derived from aircraft observations and a 1D particle growth model. Their results suggested that the retrieved N_i from the model is within an uncertainty of a factor of 2 relative to aircraft observations. But small ice crystals can easily complicate these results when their sizes are less than about $100 \, \mu m$. This shows that ice microphysical processes and snow precipitation need to be studied in more detail.

b. Remote sensing of snow measurements

Atmospheric profiling of cloud systems is important to derive accurate snow precipitation rates and to assess the cloud thermodynamical processes. The profiles of measured liquid water path (LWP), T, and RH indicate possible thermodynamical processes and can be used for validations of models and radar-based precipitation estimates. Here, the use of microwave radiometers (MWR), radars, and satellite observations to better predict snow precipitation rates are briefly summarized.

1) PMWR FOR ATMOSPHERE AND PARTICLE PHASE

A Radiometrics Corporation Profiling Microwave Radiometric (PMWR) provides continuous temperature (Fig. 6-6a), relative humidity (Fig. 6-6b), and LWC (Fig. 6-6c) vertical profiles, and integrated water vapor (IWV) and integrated liquid water (ILW) (Fig. 6-6d). These parameters can be used to better evaluate in-cloud ice processes. The PMWR includes five K-band (22–30 GHz) and seven V-band (51–59 GHz) microwave channels, a downward-looking externally mounted infrared (9.6–10.4 μm) radiometer and front-surface gold mirror assembly for cloud-base and surface
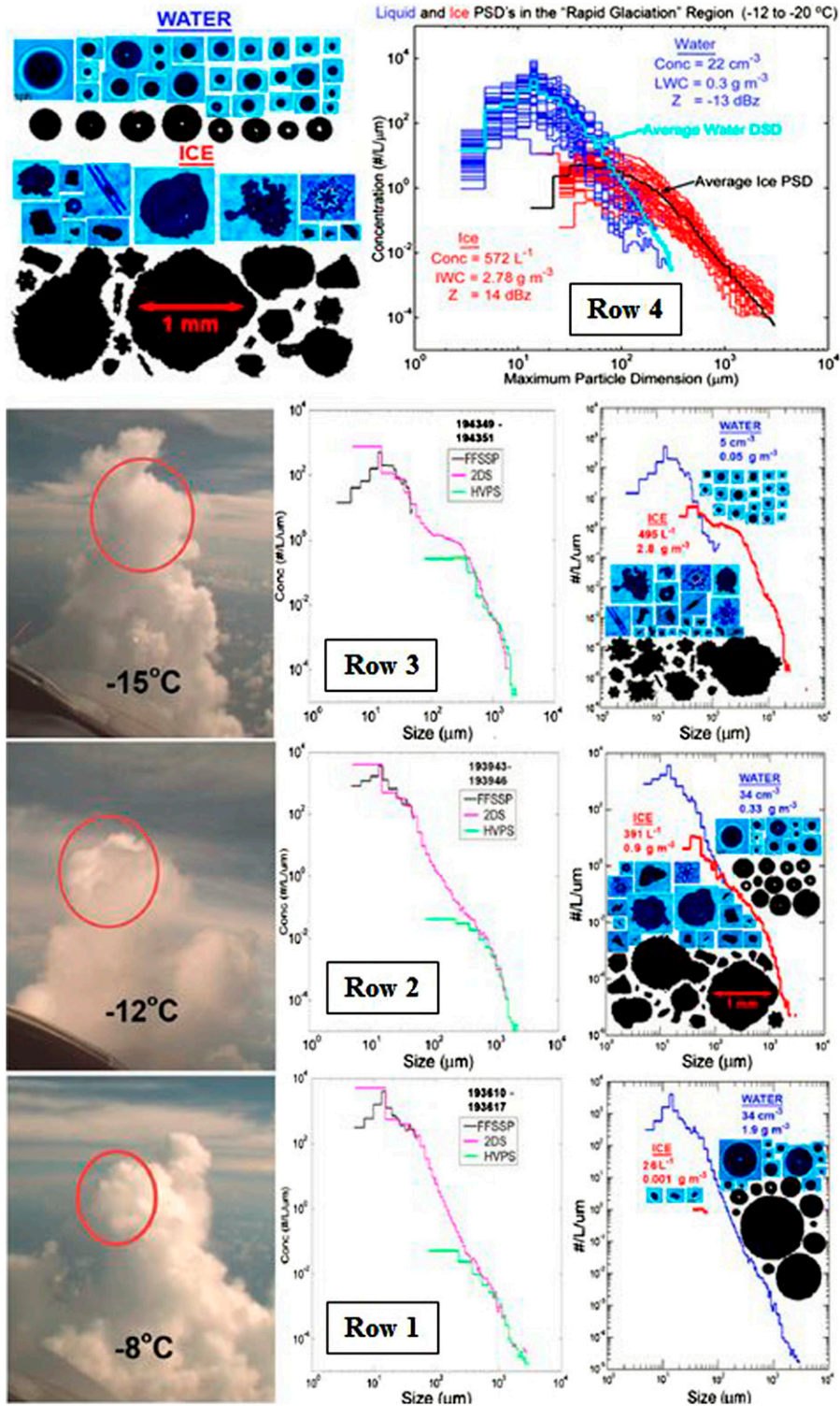
FIG. 6-5. (left) Forward-facing video photos repeated Learjet penetrations of the same cloud at three temperature levels given as −8°, −12°, and −15°C; (center) particle size distributions from three cloud particle probes (FFSSP, 2D-S, and HVPS) on the aircraft; and (right) composite size distributions of water drops (blue) and ice particles (red). Examples of Spec Inc. CPI and 2D-S images with particle number concentration (L^{-1}) and mass concentration ($g\,m^{-3}$) averaged over the updraft core are also shown in the right panels. (top left) The images of water drops and snow crystals from 2D-S probe; (top right) the particle spectra for drops and snow crystals based on CPI and 2D-S measurements (adapted from Lawson et al. 2015).
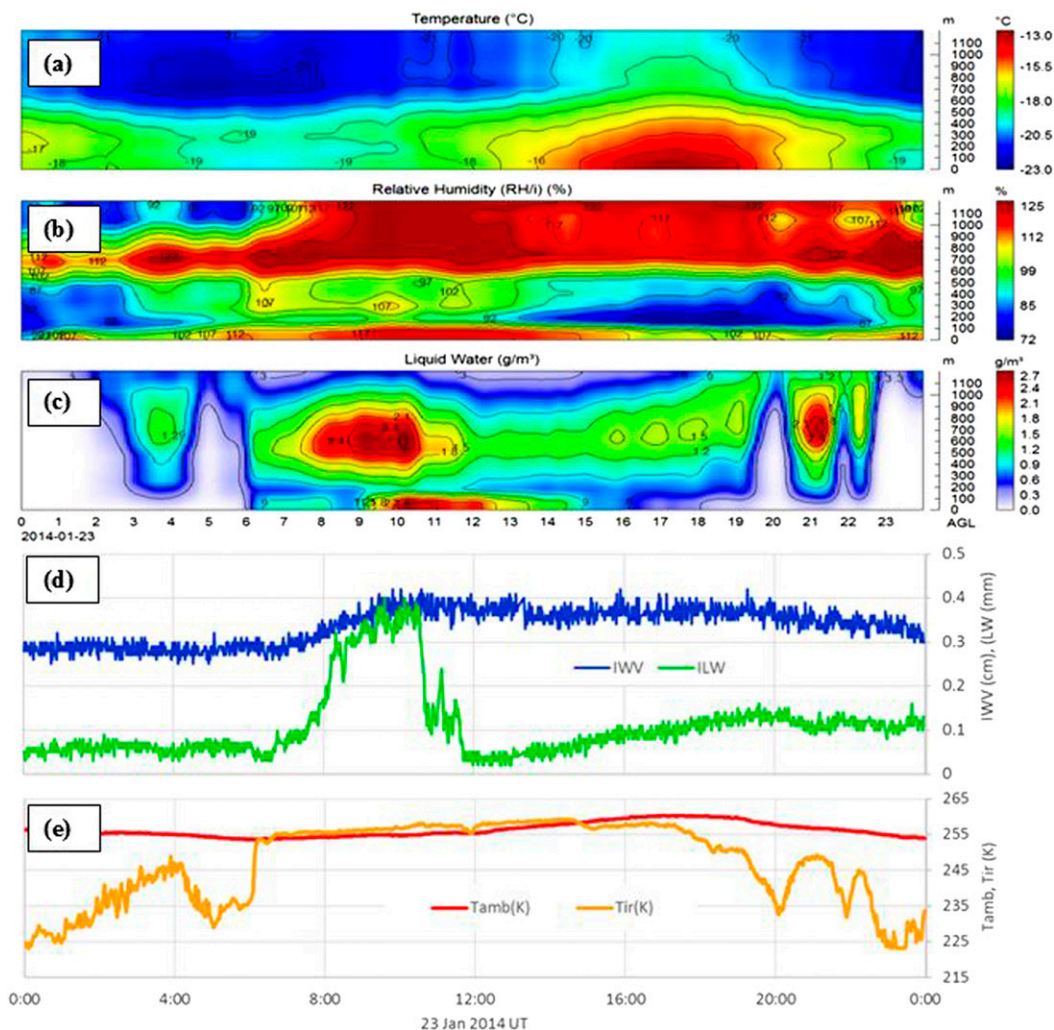
FIG. 6-6. Radiometrics PMWR (a) temperature, (b) RH over ice, and (c) LWC (×10) profile retrievals to 1.2-km height, (d) IWV and ILW retrievals, and (e) surface temperature (T_{amb}) and cloud-base IR temperature (T_{ir}) for 23 Jan 2014.

temperature estimates along with relative humidity and pressure sensors. The Radiometrics 12-channel (model MP-3000) PMWR and its performance are described by Solheim et al. (1998) and Güldner and Spänkuch (2001) and in the WMO Guide (WMO 2010; WMO/CIMO 1991). The Radiometrics model MP-3000A, introduced in 2006, includes 35 microwave channels and an internally mounted infrared sensor, providing improved accuracy and reliability (Cimini et al. 2011, 2015; Ware et al. 2013; Sanchez et al. 2013). A new W-band radar with an integrated MWR at 95 GHz has also been developed by Radiometer Physics Company for continuously deriving LWC and IWC profiles, and integrated LWP and ice water path (IWP). The Doppler and polarized capability of this integrated system can be used to better understand precipitation type and cloud system dynamics.

Background error covariance analysis shows that Radiometrics PMWR models provide better temperature and humidity profile accuracy than NWP models up to approximately 1- and 3-km height, respectively (Cimini et al. 2010, 2011, 2015). But NWPs show better accuracy at higher levels. When properly calibrated with appropriately trained neural networks, PMWRs obtain observation accuracy equivalent to that measured by radiosondes up to 10-km height (Güldner and Spänkuch 2001; Knupp et al. 2009; Cimini et al. 2011; Ware et al. 2013; Sanchez et al. 2013). The PMWR also provides 15% (Serke et al. 2014) agreement with limited independent liquid water profile and integrated liquid water measurements and estimates (Westwater 1978; Politovich et al. 1995; Turner 2007). These uncertainties can fluctuate around based on the cloud physical conditions.

TABLE 6-3. Z_e–PR_{SN} relationships are given based on earlier studies.

References	Z_e–PR_{SN}	Condition	Radar
Fujiyoshi et al. (1990)	$Z_e = 427 PR_{SN}^{1.09}$	$PR < 3 \, mm \, h^{-1}$	3.2-cm radar; 1-min gauge obs
Smith (1984)	$Z_e = 200 PR_{SN}^{1.6}$	—	Marshall–Palmer
Szyrmer and Zwadzki (2010)	$Z_e = 494 PR_{SN}^{1.44}$	—	Disdrometer
Huang et al. (2010)	$Z_e = 204 PR_{SN}^{1.58}$	—	2DVD

2) RADAR-BASED PRECIPITATION RETRIEVALS

Radars that use various transmission wavelengths have been used for many years for research on cloud microphysics and snow precipitation (Sekhon and Srivastava 1970; Wolfe and Snider 2012; Ryzhkov et al. 2011; Jung et al. 2010; Lang et al. 2011). Reflectivity–snowfall rate relationships to obtain snow amount at the surface are usually expressed in terms of a power law (Wolfe and Snider 2012) as

$$Z_e = \alpha PR_{SN}^{\beta}, \qquad (6\text{-}7)$$

where Z_e (mm^6 m^{-3}) is the equivalent radar reflectivity factor and PR_{SN} (mm h^{-1}) is the snowfall rate, representing the liquid equivalent amount per unit time. The coefficients α and β are estimated by correlating Z_e and PR_{SN} either observed directly or computed from measurements of the particle size distribution. Assuming an exponential snow precipitation size distribution, based on Rasmussen et al. (2003), Wolfe and Snider (2012) provided a relationship between Z_e and PR_{SN} as

$$Z_e = \left(22.2 \frac{K_i^2}{K_w^2} \frac{\rho_w^{5/3}}{\rho_i^2} \frac{\Omega^{1/3}}{V_t^{5/3} n_o^{2/3}} \right) PR_{SN}^{5/3}, \qquad (6\text{-}8)$$

where K_w and K_i are dielectric factors for droplets (0.18) and ice crystals (0.93), respectively, at the S band. The ρ_w and ρ_i are water and ice densities given by 1 and 0.92 g cm^{-3}, respectively. The n_o and Ω are the intercept parameter based on exponential size distribution of snow particles and an assumed constant (Wolfe and Snider 2012), respectively. In the derivation of Eq. (6-8), several empirical relationships associated with the assumed particle size distribution are used. Alternatively, Wolfe and Snider (2012) derived another relationship similar to Eq. (6-8) based on S-band radar measurements, but n_o is replaced with N_i (total particle number concentration). Further, using an ice dielectric constant proportional to the ice-water surface density and $\rho_i = \Omega/D$, Z_e is obtained as

$$Z_e = \left(21.9 \frac{K_i^2}{K_w^2} \frac{\rho_w^2}{\rho_i^2} \frac{1}{V_t^2 N_i} \right) PR_{SN}^2. \qquad (6\text{-}9)$$

These relationships can be used to obtain PR_{SN} when the particle size distribution and V_t of snow crystals are known accurately, and these relationships can change based on the various radar transmitting channels. The errors increase with large PR for radars with $x = 3.2$ cm. Some other Z_e–PR relationships obtained from observations are given in Table 6-3.

Equations given in Table 6-3 can be used to estimate PR_{SN} values from radar-based Z_e observations but these relationships become more complicated in the melting layers where ice crystals and snow particles melt when T becomes more than or equal to 0°C. Uncertainty related to Eqs. (6-8) and (6-9) is due to assumed spherical geometry for snow and mass–density relations. To overcome these issues, Mitchell et al. (2006) suggested use of mass–dimensional power law to define the particle polarizability. Then, using the size distribution parameters and m–D power-law relationship approach, they estimated IWC as a function of Z_e, and that can be used for PR_{sn} calculation obtained from the product of IWC and particle fall velocity V_f. Although this method works for NWPs model applications, it will be difficult to apply for radar observations because of assumed PSD and m–D relationships.

Integrated methods are now being used for precipitation research, for example, using a 94-GHz W-band radar, lidar, and *CloudSat* radar, as well as an NWP model approach based on bulk and bin microphysical algorithms. Iguchi et al. (2012) simulated convective clouds that formed over the northwest Pacific of Japan during 14–28 May 2001 (Fig. 6-7). Bin-based microphysical simulations based on Japan's Japan Meteorological Agency Nonhydrostatic Model (JMA-NHM) operational 3D-forecast model were compared using various microphysical algorithms. Significant differences among the methods were found, with the bin-based simulations providing much more detail on the precipitation processes, including the fall velocities of each particle shape (droplet, columns, plates, dendrite, snow, graupel, and hail). Ferrier (1994) used a gamma size distribution function to represent the size distributions of various ice crystal types and rain, and predicted two moments of four different classes of bulk hydrometeors. In his calculations, the intercept, the slope, and shape parameters are
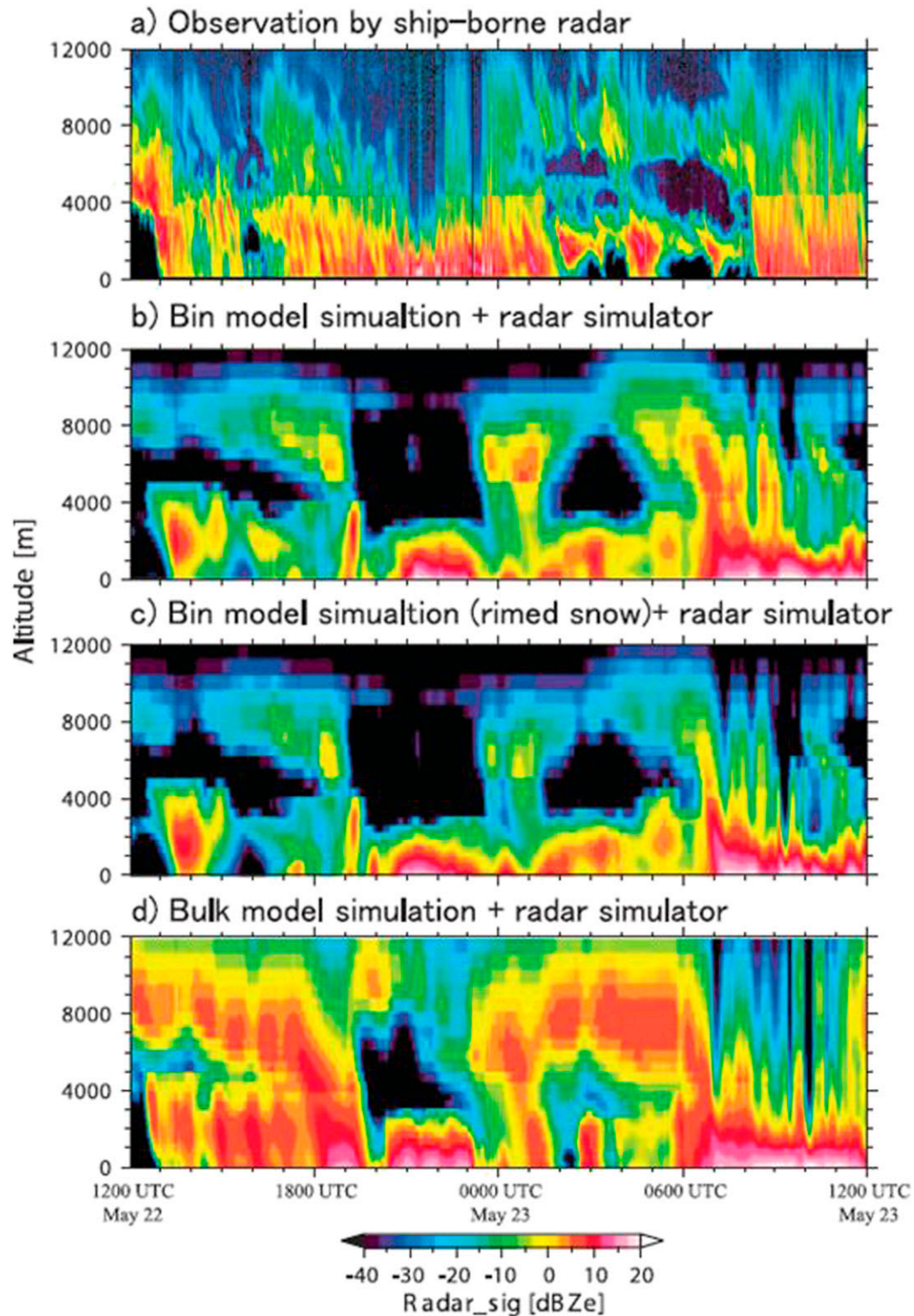
FIG. 6-7. Time–height cross sections of the equivalent radar reflectivity factor (dBZe) (a) measured by the 95-GHz Doppler radar on board the Mirai ferry, and calculated by the radar product simulator applied to the outputs of (b) the bin (control) simulation, (c) the bin with the terminal fall velocities of snow equalized to those of hail in all size bins (rimed snow), and (d) the bulk model simulations from 1200 UTC 22 May to 1200 UTC 23 May 2001 (adapted from Iguchi et al. 2012).

calculated for each particle type, and then mixing ratio and number concentration are retrieved. He stressed that interacting particle distributions within the cloud should be preserved rather than only number concentrations. Iguchi et al. (2012) compared the radar reflectivity factors derived using four different combinations of observations with NWP model predictions of radar reflectivity. Their results are shown in Fig. 6-7. This figure suggests that riming processes and bulk versus bin microphysics schemes resulted in significant difference in reflectivity factor Z_e. They also stated that substantial uncertainties in the mass–size and size–terminal fall velocity relations of snowflakes significantly affected the results. For the bulk microphysics, they stated that overestimation of Z_e was likely due to substantial deposition growth directly onto snow that was not modeled using the bin scheme.

During the last couple of decades several studies in the literature have focused on retrievals of ice particle properties with polarimetric radars (Zhang et al. 2011a,b; Hogan et al. 2003; Ryzhkov and Zrnic 2007). Polarimetric radar observations can be used to detect cloud physical properties, for example, particle phase, shape, and water content, and hence derive information about processes that play an important role for snow precipitation (Kennedy and Rudledge 2011). Bechini et al. (2013) used observations from C- and X-band radars in northwestern Italy to study the behavior of the polarimetric variables in the ice region of precipitating stratiform clouds, with special emphasis on the specific differential phase parameter K_{dp}. They state that stratiform precipitation, irrespective of the precipitation type at the ground and as opposed to convective systems, is characterized by well-pronounced positive differential reflectivity Z_{dr} and K_{dp} values near the model-predicted $-15°C$ isotherm (Fig. 6-8). This figure shows the profiles of various polarimetric parameters, including horizontal reflectivity Z_h, Z_{dr}, K_{dp}, and correlation coefficient ρ_{HV} as a function of T for stratiform and convective clouds. The regions of enhanced Z_{dr} and K_{dp} are likely related to the growth of dendrite crystals in the area where the difference between the saturation vapor pressure over water and the saturation vapor pressure over ice is greatest. Yuter and Houze (1995) defined a metric for convection called the radar convective parameter (RCP; a simple parameter to describe the degree of convection in a given reflectivity vertical profile) that is also plotted on this figure. Bechini et al. (2013) defined stratiform conditions when RCP is lower than the 50th percentile and is convective otherwise. Their work also showed, in stratiform precipitation, that K_{dp}

observations around the $-15°C$ temperature level are well correlated (0.8) with the reflectivity in the underlying rain layer.

3) SATELLITE-BASED PRECIPITATION RETRIEVALS

Cloud and snow retrievals can be performed based on active sensors on satellites, for example, radars or direct measurements of satellite passive spectral channels (Matrosov 2015; Matsui et al. 2013; Iguchi et al. 2012; Rabin et al. 2016). Iguchi et al. (2012) indicated a relatively high correlation of around 0.7 between satellite and WSR-88D IWP retrievals. The mean relative differences between spaceborne and ground-based estimates of IWP were around 50%–60%, which is on the order of IWP retrieval uncertainties and is comparable to the differences among various operational *CloudSat* IWP products. IWP is an important ice cloud parameter that is routinely retrieved from *CloudSat* measurements and used to characterize the quantitative evolution of precipitating ice regions. IWP can be estimated in predominantly stratiform precipitation systems that are characterized by a radar bright band, which effectively separates the precipitating ice cloud regions from layers containing rain. The bright band is defined as the cloudy layer where melting and aggregation of ice or snow crystals increases at about 0°C, resulting in large reflectivity for melting snow. This happens because of water's reflectivity is approximately 9 or 10 times as reflective as ice for the microwave energy range. Therefore these large wet snowflakes will show a high reflectivity (Caylor et al. 1990; Harrison et al. 2000) that needs to be corrected for accurate precipitation rate–reflectivity relationships.

Multispectral infrared observations obtained from *Geostationary Operational Environmental Satellite-13* (*GOES-13*) can also provide estimates of snowfall on the ground (Rabin et al. 2016). In their work, a new technique is described for identifying clouds capable of producing high snowfall rates and incorporating wind information from the satellite observations. The potential for monitoring snowfall at the surface from estimates of cloud-top temperature and height, phase (water, ice), hydrometer size, optical depth, inferred altitude of the dendritic ice growth zone, horizontal wind patterns near cloud tops, and a GOES precipitation algorithm are evaluated. The time evolution of these satellite estimates are validated using measurements obtained from ground-based in situ and remote sensing platforms during both precipitation events.

The Global Precipitation Measurement (GPM) satellite, based on Ku- and Ka-band radars, as well as microwave sensors, provides next-generation satellite-based precipitation measurements and a better understanding of energy/water cycles in the weather and climate system (Matsui et al. 2013; Li et al. 2005;
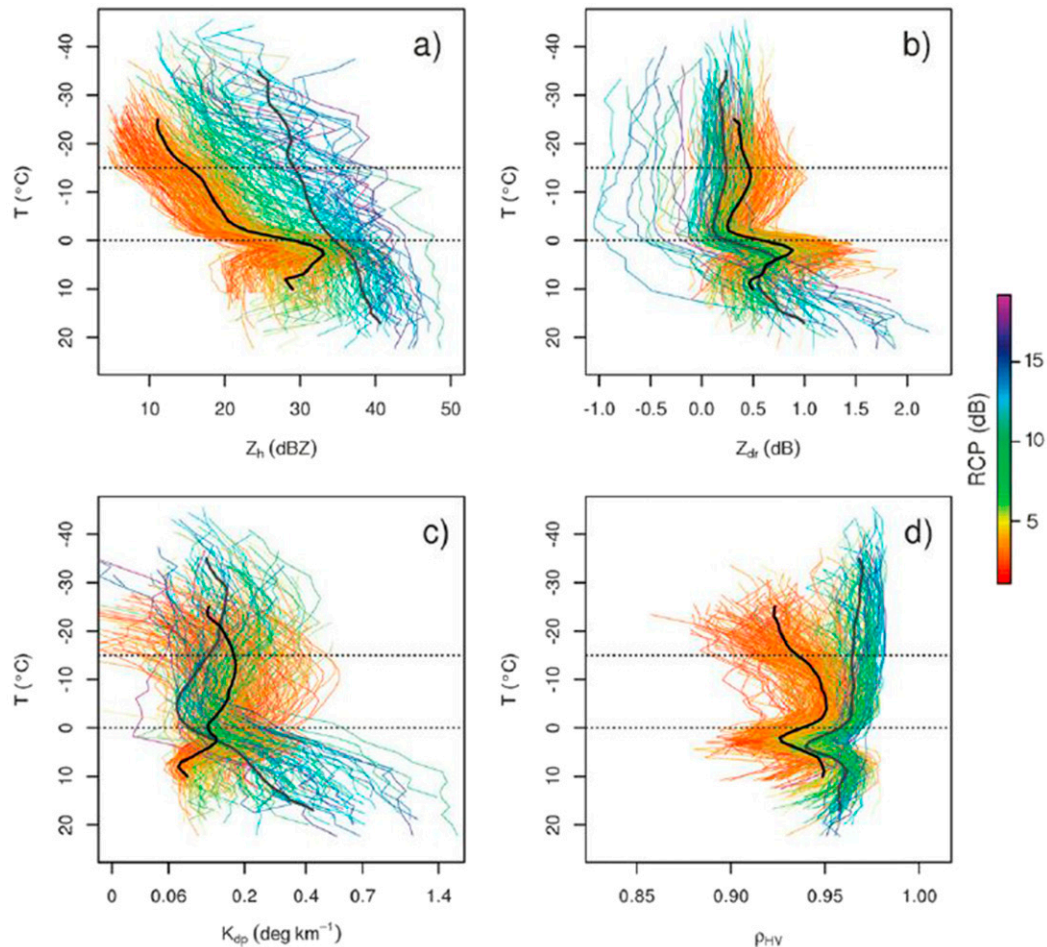
FIG. 6-8. Hourly vertical profiles of C-band (a) horizontal reflectivity Z_h, (b) differential reflectivity Z_{dr}, (c) differential phase shift K_{dp}, and (d) correlation coefficient ρ_{HV} colored according to their respective RCP values. The RCP quantiles (0%, 25%, 50%, 75%, and 100%) represent values of 1.1, 2.7, 3.9, 7.3, and 21.7 dB, respectively. The black (gray) thick lines represent the average of the daily profiles for stratiform (convective) events. To highlight the variations for small values, the K_{dp} profiles are plotted on a log axis (adapted from Bechini et al. 2013).

Atlas et al. 1995). To meet accuracy requirements, the GPM *Core Observatory* satellite carries a combination of active and passive microwave sensors with improved capabilities to detect light rain and falling snow. A dual-frequency Precipitation Radar (DPR) on the GPM satellite provides radar observations at both Ku band (13.6 GHz) and Ka band (35.5 GHz) and includes a high sensitivity mode for detection of light/frozen precipitation (Fig. 6-9). The GPM Microwave Imager (GMI) includes 10–89- and 166–183-GHz channels (Fig. 6-9). These sensor upgrades require more complex precipitation algorithms that harness multisensory and multifrequency satellite signals to estimate warm-/cold-/mixed-phase precipitation rates over various precipitation regimes. The GPM simulator, which is based on forecasting

model products, can be used as a tool for radiance-based precipitation microphysics evaluation and assimilation methods (e.g., Matsui et al. 2009; Li et al. 2010; Han et al. 2013). The GPM satellite simulator translates the Weather Research and Forecasting Model with Spectral Bin Microphysics (WRF-SBM) simulated geophysical parameters (Iguchi et al. 2012; Li et al. 2005) into the GPM satellite products for validation applications. The WRF-SBM features explicit size-bin-resolving cloud microphysics rather than the bulk microphysics used in the previous satellite applications.

5. Snow precipitation prediction

In this section, processes and issues related to snow prediction based on numerical models are summarized.
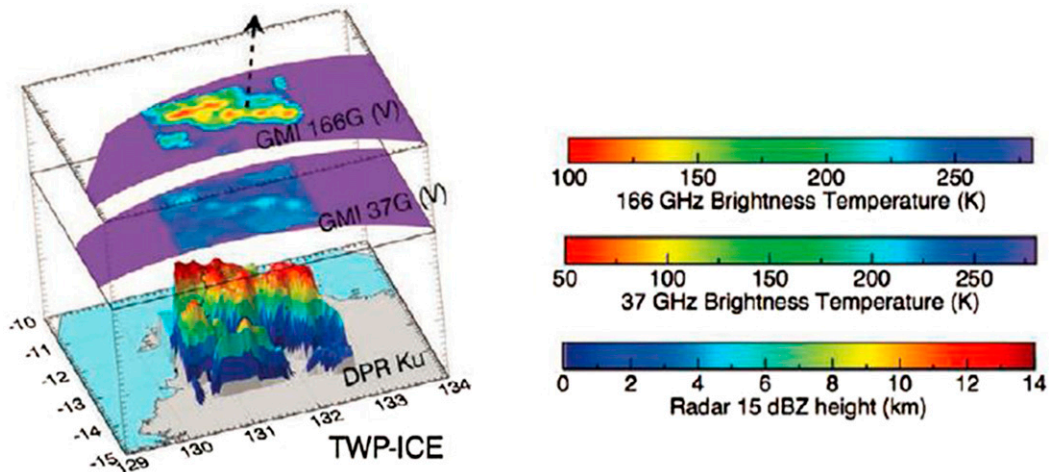
FIG. 6-9. 3D view of the simulated GPM orbital data over the Tropical Warm Pool–International Cloud Experiment (TWP-ICE) project location. Color-shaded terrain represents 15-dBZ echo-top height of the DPR Ku band, and horizontal slices of color shades represent microwave brightness temperature of the GMI 37- and 166-GHz (V) channels (adapted from Matsui et al. 2013).

a. Processes affecting snow precipitation

Cloud microphysical processes determine the type and amount of precipitation at the surface. Although there have been significant developments over the last 50 years, it is still challenging to predict cloud microphysics properties and snow precipitation with forecasting models because of the issues related to measurements used to derive physical parameterizations. The major issues with snow precipitation involve in-cloud microphysical processes such as ice nucleation, ice crystal growth, collision–aggregation processes, riming, secondary ice crystal production, and freezing and melting, as well as dynamical processes such as mixing and turbulence.

Ice nucleation [see Kanji et al. (2017, chapter 1) and Gultepe et al. (2017, chapter 4)] parameterizations have important effects on PSDs that occur mainly in two ways: (i) heterogeneous nucleation and (ii) homogeneous nucleation (Gultepe et al. 2016). There are different mechanisms by which heterogeneous nucleation occurs as follows: 1) deposition/freezing nucleation, 2) contact nucleation, 3) immersing nucleation, and 4) secondary ice nucleation. Homogeneous nucleation happens at temperatures less than about −38°C. Heterogeneous nucleation occurs because of the existence of INPs that can affect the precipitation amount and rate at the surface. Anthropogenic aerosol can also potentially play a role as heterogeneous ice nucleating particles and affect precipitation For instance, increasing INP concentrations may lead to more but smaller ice crystals (for the same ice water content) that suppresses snow amount but increases cloud cover (Zubler et al.

2011; Saleeby et al. 2013). On the other hand, for the case of reduced INP concentration within convective clouds, aerosols can play a different role, potentially leading to increasing precipitation (Rosenfeld and Lensky 1998; Williams and Stanfill 2002; Xu 2013) as a result of newly formed ice crystals, followed by collision–coalescence and aggregation processes. Secondary ice production (Field et al. 2017, chapter 7) can also modify the PSD through the production of large numbers of small ice crystals.

The uncertainties associated with the in-cloud sedimentation of hydrometeors are related to the microphysical characteristics of solid and liquid water particles such as particle size, habit, and water amount. These parameters are related to particle terminal velocity and mass, as well as updrafts and turbulence. In convective clouds, vertical air velocity and turbulence play a major role in particle growth as they impact both riming and aggregation while they grow by vapor diffusion (Kajikawa and Heymsfield 1989). Particle densities are related to particle habit and temperature that affect precipitation type, rate, and amount extensively. Precipitation in NWPs and cloud models occurs as a function of the assumed threshold value of crystal size and/or IWC (or LWC) in a model process that is called autoconversion and that represents the coalescence of small cloud particles (ice or liquid) to form larger precipitation-sized particles. During an autoconversion process, excessive cloud water or cloud ice beyond the threshold values is converted to falling snow (Gultepe et al. 2016). For autoconversion of cloud water to rain, it is usually assumed that droplets are larger than 40–50 μm, whereas for autoconversion of ice crystals to snow, ice crystals are

assumed to be larger than 200–500 μm (Khairoutdinov and Kogan 2000; Gultepe et al. 2015). The representation of autoconversion processes in NWP and climate models are still subject to large uncertainty especially for snow precipitation, and needs to be better evaluated. In the last section in this chapter, this issue will be clarified with new suggested methods that focus on the prediction of the evolution of particle properties (e.g., Harrington et al. 2013a,b; Morrison and Milbrandt 2015).

b. Prediction of snow precipitation

Numerical modeling of snow precipitation can be challenging because of the complex microphysical processes that occur within cloud systems. Assumptions used in microphysical parameterization algorithms in NWP and climate simulations should be tested by comparing observations and model simulations.

The majority of microphysics parameterizations can be classified based on how they treat the size distribution for each particle category. Bin-resolving schemes discretize the PSD of each hydrometeor category into a finite number of size or mass bins and predict changes to the distribution by predicting changes to the number (and sometimes also mass) of particles in each bin. No functional form of the PSD is assumed and if the number of bins is large enough, details of the PSD can be well resolved. The driving model must advect the predicted number (and mass) in each bin. Bin schemes are very computationally expensive, particularly in 3D models, and with current computational power, they can only be used in research mode.

For the bulk microphysics approach, each PSD is assumed to have a specific functional form, such as a gamma distribution or lognormal distribution. Many schemes assume a three-parameter complete gamma distribution (which reduces to an inverse-exponential distribution for a shape parameter value of zero). Changes to the PSD are modeled by predicting changes to one or more parameters that describe the function. One or more moments of the distribution are then predicted, which in turn result in changes to the distribution parameters. For each prognostic moment, there is a degree of freedom (i.e., an independently varying PSD parameter). The changes to the moments are computed as the sum of the changes due to each parameterized microphysical processes where each process rate is essentially computed by taking the growth rate for a particle of a given size or mass, multiplying by the PSD, integrating over all sizes, and relating the integral quantity to the prognostic moment. The prognostic moments are normally related to physical quantities such as the total mass or number

concentration; other quantities such as reflectivity can also be used in a similar way. Because of the reduced number of prognostic variables used in bulk microphysics schemes compared to bin schemes, and the low cost of computational advection and diffusion used by the dynamical model, as well as the schemes themselves, bulk schemes (Tiedtke 1993; Del Genio et al. 1996; Sundqvist et al. 1989) in operational NWP and climate prediction models are preferred for precipitation prediction relative to detailed bin microphysics schemes (e.g., Onishi and Takahashi 2012).

The PSDs of precipitation particles such as rain, snow, and graupel are usually assumed to have a simple exponential form (Iguchi et al. 2012), as

$$N(D) = N_o \exp(-\lambda D), \tag{6-10}$$

where D is the particle diameter, λ the slope parameter, and N_o is the intercept parameter. The mass and terminal velocities for each particle type are described as a function of particle diameter. Eito and Aonashi (2009) used two-moment bulk microphysics scheme to study frozen hydrometeor properties simulated by the JMA-NHM and calculated the slope parameter as

$$\lambda_{S,R,G} = \left(\frac{\pi \rho_s N_{oS,R,G}}{\rho_a q_{S,R,G}} \right)^{0.25}, \tag{6-11}$$

where q is the mixing ratio with subscripts for snow (S), rimed particles (R), and graupel (G), ρ_a is the air density, and ρ_s is the snow density. The N_o is the prescribed number concentration of particles or it can be obtained through the slope parameter when an exponential PSD is assumed. The D parameter is usually defined in terms of maximum size of ice crystals when ice microphysical parameters are determined (McFarquhar and Black 2004). The empirical equations for mass–size relationships are usually prescribed; therefore, they need to be specified for various particle types. In addition to processes of vapor diffusion and ice nucleation, accretion, collision and coalescence, riming, breakup, and aggregation processes through autoconversion, affect the amount of falling snow. The presentation of all of these processes use constant coefficients that are poorly known.

The total production of snow needs accurate estimates of both source and sink terms for vapor and water related parameters. These parameters are related to in-cloud microphysical processes (Lin et al. 1983; Ferrier

TABLE 6-4. The main source and sink terms as subscripts used in the water budget equation [Eq. (6-12)] to estimate snow precipitation amount P.

SAUT	Autoconversion of cloud ice to snow
SACI	Accretion of cloud ice by snow
SACW	Accretion of cloud water by snow
SWF and SFI	Rates at which cloud water and cloud ice transform to snow by deposition and riming, respectively, based on the growth of a 50-μm ice crystal
RACI	Accretion of cloud ice by rain
IACR	Accretion of cloud ice by rain
GACS	Accretion of rain by graupel
GAUT	Autoconversion of snow to graupel
RACS	Accretion of snow by rain
SACR	Accretion of rain by snow
SSUB	Sublimation lost from the snow
SDEP	Depositional growth of snow

1994) that represent the mass conservation of snow (SN) crystals as

$$P_{SN} = P_{SAUT} + P_{SACI} + P_{SACW} + P_{SFW} + P_{SFI} + P_{RACI}$$
$$+ P_{IACR} + P_{GACS} + P_{GAUT} + P_{RACS} + P_{SACR}$$
$$+ P_{SSUB} + P_{SDEP}.$$
$$(6\text{-}12)$$

All the components for snow production [Eq. (6-12)] such as ice nucleation, vapor diffusion, aggregation, riming, and autoconversion are described in Table 6-4 and are based on several assumptions related to their physical characteristics (e.g., mass–length relationships, particle size distributions, fall velocities, collection efficiencies); hence, these play an important role for snow precipitation prediction (Tomita 2008). All of the processes given in Eq. (6-12) can be formulated as proportional to moments of the snow size distribution. Some approaches simply use prognosed moments such as ice water content combined with atmospheric variables such as temperature (for a single-moment scheme) to directly predict the moments required for each process. In this way the PSD information is implicit in moment prediction equations (Thompson et al. 2008; Field et al. 2007).

6. Precipitation efficiency

Precipitation efficiency [P_{eff} (h^{-1})] is defined by the ratio of the observed precipitation on the ground to the possible precipitation flux within the cloud that is the product of total water content (TWC; excluding vapor amount) and V_f, representing the entire cloud system (Sui et al. 2007; Gultepe 2015). Here, it is defined as

$$P_{eff} = \frac{PR}{V_f \, TWC} \frac{C}{\Delta t}, \qquad (6\text{-}13)$$

where PR (kg m^{-2} h^{-1}) is the precipitation rate at the surface, TWC (kg m^{-3}] is the total condensed water content, V_f (m s^{-1}) is mass concentration weighted fall velocity within the cloud, C is the conversion factor for time (1/3600), and Δt (h) is the time period. Note that this ratio has units of inverse time. Therefore it represents the reciprocal of the time scale to remove condensed water via precipitation. The P_{eff} can change as a function of numerous atmospheric parameters. The P_{eff} deviates from values that would be expected based on adiabatic conditions. For example, P_{eff} can change from 10% up to 70% except for highly saturated orographic convective systems where it becomes nearly 100% as pointed by Browning et al. (1974, 1975) and Schmidt (1991). P_{eff} can be calculated differently based on the need of application and some of them are presented below.

Precipitation rate over the orographic areas can be related to the various factors including mountain physical conditions and meteorological parameters. The studies of Jiang and Smith (2003), Sawyer (1956), and Elliott and Hovind (1964) suggested that P_{eff} can change from 20% up to 100% dependent on environmental conditions. Precipitation efficiency over the orographic areas can be influenced by mountain topography in addition to meteorological parameters. Variability in weather conditions over mountainous regions can be significant for the short distances along the mountain slopes. Liquid or solid precipitation amount over the slopes may increase or decrease with height, depending on how the thermodynamic conditions and atmospheric stability change along these slopes (Gultepe et al. 2015; Gultepe and Zhou 2012; Mo et al. 2014). Knuth et al. (2010) suggested that blowing and drifting snow plays very important roles on the snow depth measurements. They stated that more than half of their observation sites were influenced by these factors and hence precipitation measurements included large uncertainties. Similar issues related to blowing and drifting snow effects on precipitation measurements were also stated by Choularton et al. (2008), Rogers and Vali (1987), and Lloyd et al. (2015).

The measurements of meteorological parameters such as precipitation type, amount, intensity, and phase changes along the mountain slopes also play an important role in assessing the model-based predictions of P_{eff}. The model resolution plays an important role for precipitation rate because of inhomogeneity in its distribution (Mailhot et al. 2014). The lower precipitation amounts usually occur with decreasing resolution in the model, and forecasts precipitation rate decreases with increasing grid area size. They

pointed out that sampling strategies are important for model validation studies and precipitation assessment. Therefore, the model simulations should be done with the appropriate time and space scales, resolving the physical processes. Jiang and Smith (2003), using a mesoscale numerical model with a 3D Gaussian-type mountain called Advanced Regional Prediction System (ARPS), studied P_{eff} over an orographic region. If $\hat{s}_c$ represents an assumed specific condensate rate and $\hat{s}$ the measured condensate rate, then $R(\hat{s}_c/\hat{s})$ (Jiang and Smith 2003) is provided as

$$R = \gamma \frac{\sqrt{\pi q_{vs}(0) h_m}}{D(\tau_a^{-1} + \tau_f^{-1})}, \qquad (6\text{-}14)$$

where D is the model box height, τ_f is the fallout time scale, γ is the collection factor, τ_a is the advection time scale, $q_{vs}(0)$ is the saturation vapor mixing ratio at the surface, and h_m is the mountain height. Assuming these as $1\,km$, $1000\,s$, $0.5\,s^{-1}$, $1000\,s$, $2\,g\,kg^{-1}$, correspondingly, the critical h_m should be $500\,m$ to make $R = 1$ (Jiang and Smith 2003). Changing from a nonprecipitating to precipitation stage, R should increase by either decreasing $\hat{s}_c$ or increasing $\hat{s}$ as suggested by Jiang and Smith (2003). A relationship between P_{eff} and R over the windward side of the mountain is given as

$$P_{eff} = \frac{1 - \dfrac{1}{R}}{1 + \dfrac{\tau_f}{\tau_a}}. \qquad (6\text{-}15)$$

The results obtained based on Eq. (6-15) suggest that P_{eff} increases from 0% to 40% with increasing R from 1 to 5, nonlinearly. The value of R can increase by mountain height, q_{vs}, advection time, increasing collection factor, fallout time, increasing horizontal wind speed, and decreasing mountain width.

The P_{eff} can also be defined based on modeling needs such as obtaining precipitation intensity from a forecast model. Braham (1952) used the influx of water vapor into the storm base as the rainfall source, and defined it as the ratio of PR to the sum of precipitation source terms, representing large-scale precipitation efficiency (LSP$_{eff}$). This definition as indicated by Li and Gao (2011) is used by many others in the forecasting models (Ferrier et al. 1996; Tao et al. 2004; Sui et al. 2005; 2007), and details of this subject can be found in Li and Gao (2011). Based on cloud microphysical schemes, P_{eff} using microphysical budget source terms (Sui et al. 2005) is also defined as cloud microphysics precipitation efficiency (CMP$_{eff}$) (Li et al. 2002; Sui et al. 2005). Snow precipitation efficiency, as described in budget terms for snow precipitation, can also be defined similarly.

7. Snow precipitation effects on weather, climate, and society

In this section, snow precipitation effects on weather, climate, and society are studied.

a. Weather

Snow precipitation is an important parameter affecting weather processes within and below the cloud. It affects visibility, temperature, and surface weather conditions such as flooding and cooling processes. Its intensity at the surface is related to falling snow crystal size and habit distributions, as well as particle fall velocity. For example, snow intensity can be parameterized based on characteristic snow crystal size, crystal density, and Vis (Gultepe et al. 2016) as

$$PR_{SN}\,(mm\,h^{-1}) = A\rho_i D_o V_t/Vis, \qquad (6\text{-}16)$$

where A is 4.68×10^4 and D_o is the median diameter. This equation is similar to that of Rasmussen et al. (1999). The effect of snow precipitation on visibility is crucial for aviation and transportation applications (Gultepe et al 2014a; Stoelinga and Warner 1999). Figure 6-10 shows Vis versus snow PR$_{SN}$ observations for various particle shapes based on ground-based FD12P present weather sensor observations. The fit equation given in the figure with standard deviations indicates the variability of Vis versus PR for various snow types.

To assess the SN impact on weather processes, the energy equivalent of PR can also be considered. According to the energy conservation budget, a relationship between PR$_{SN}$ (mm day^{-1}) and its equivalent energy amount Q_e (W m^{-2}) due to sublimation can be obtained as

$$Q_e = K_c PR_{SN} L_{ice}, \qquad (6\text{-}17)$$

where K_c is a conversion constant of $1/86\,400$ day, and L_{ice} (J kg^{-1}) is the latent heat of sublimation. When the surface is covered by snow, energy taken from surrounding air for evaporation of ice crystals (sublimation) is more than required for a surface covered by water (Barry 1981). Using L_{ice} at 0°C as 2.83×10^6 J kg^{-1} and assuming PR $= 1$ mm day^{-1} occurring over the Arctic regions, Q_e becomes 32.8 W m^{-2}. This suggests that latent heat is released at cloud levels by condensation and consumed by sublimation of snow crystals at the surface. Both effects modify the outgoing infrared radiative fluxes that result in net cooling at the surface.

b. Climate

Snow precipitation affects the hydrological cycle and climate budget terms, for example, surface heat and
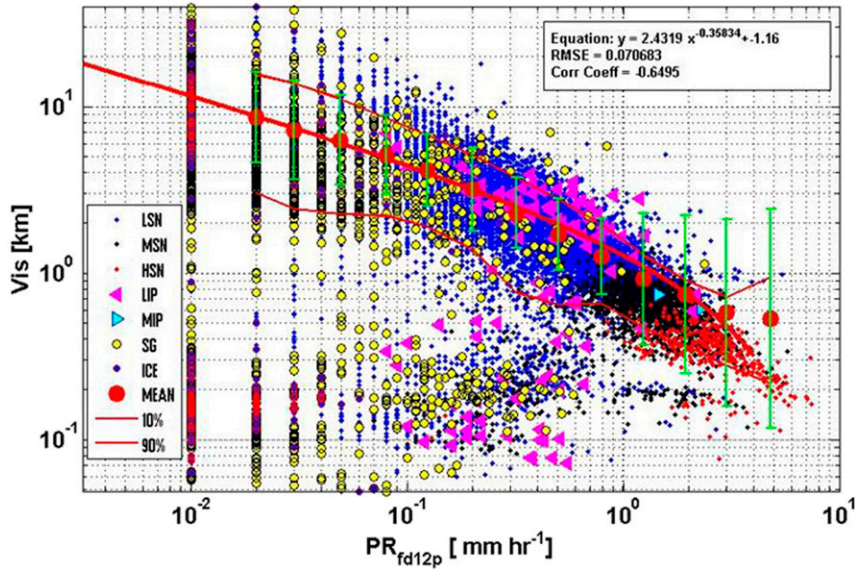
FIG. 6-10. FD12P Vis vs PR for all snow events occurred during the FRAM Science of Nowcasting Winter Weather for Vancouver 2010 (SNOW-V10) project for various precipitation types shown in the legend (adapted from Gultepe et al. 2014a,b). The symbols as LSN, MSN, HSN, LIP, MIP, SG, and ICE represent light snow, moderate snow, heavy snow, light ice crystal precipitation, snow grains, and ice crystals, respectively.

moisture budgets, and cloud water budget terms. Ice clouds in the atmosphere can modify IR heating and cooling profiles. Falling snow crystals results in cooling at higher levels after decreasing cloud amount (dehumidify the cloud layer) and IR cooling at the surface. Evaporative cooling at the surface due to absorption of heat from environment also occurs. Observations collected by snow precipitation sensors can be used to provide climatological trends after removal of wind effects. A LPM disdrometer during the entire SAAWSO project, which took place in the sub-Arctic, was used to assess the LSN impact on snow occurrence (Gultepe et al. 2016). Figure 6-11 shows a probability density function (pdf) plot for PR_{SN} over the entire SAAWSO project that includes heavy snow (HSN) conditions that occurred over an ~1-yr time period, representing winter conditions (Gultepe et al. 2016). The fit equation for the pdf of snow PR based on the Weibull distribution is obtained as

$$\text{pdf} = 0.2\frac{a}{b}\left(\frac{x}{a}\right)^{b}e^{-x^{b}/a}, \tag{6-18}$$

where x is the PR, $a = 0.3407$, $b = 0.67$, and 0.2 is the normalization factor for the fit. Figure 6-11 suggests that LSN PR < 0.5 (1.0) mm h^{-1} occurred 75% (87%) of the time and the corresponding PA represented 11% (20%) of the total.

The global distribution of snowfall is very important for climate studies because of its effect on the hydrological cycle (Löhnert et al. 2011; Tapiador et al. 2012), and it is strongly related to climate change. Low precipitation

rates, low temperatures, and strong wind effects can make accurate snowfall measurements a challenge. Previous studies (Rasmussen et al. 1999; Gultepe et al. 2015) suggested that the main challenges in adequately measuring snowfall are the high spatial and temporal
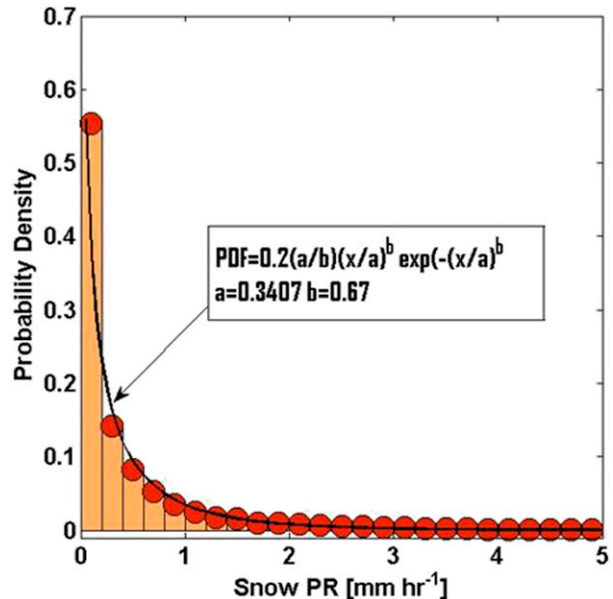

FIG. 6-11. Histogram of PR for the entire SAAWSO project that took place over Goose Bay, NL, Canada, from 1 Nov 2013 to 1 May 2014. The pdf of PR is obtained based on Weibull distribution function given by Eq. (6-22), which is shown on the figure.

variability as well as the enormous complexity of snow crystal habit, density, and PSD. Accurate surface-based snowfall measurements are only sporadically available in the northern regions. Therefore, satellite remote sensing methods are needed to estimate LSN amount and rate but these methods lack sensitivity to low LSN PR.

Global precipitation measurements, including methods, uncertainty, datasets, and applications related to snow measurements, were studied by Gruber and Levizzani (2008), Rudolf and Rubel (2005), and Tapiador et al. (2012). These studies concluded that LSN measurements and its prediction may include large uncertainties that can affect validation of model simulations with observations. Figure 6-12 shows that precipitation changes are up to 50% in many regions of world, and it is likely that climate change will result in quick melting of snow on the ground; therefore, snow science and research need to be further explored for polar conditions.

Overall, snow precipitation processes are important for climate change assessment, the hydrological cycle, NWP model validations, and aviation applications. The LSN (defined as PR $< 0.5\,\mathrm{mm\,h^{-1}}$) precipitation in cold climates usually cannot be measured accurately because of instrumental issues; sensor calibrations unavailable for cold weather conditions, and unreliable response of the optical sensors to the cold and harsh environments (Gultepe et al. 2016).

c. Society

Snow precipitation can affect society through the interruption of commercial flights (Gultepe et al. 2016; Rasmussen et al. 1999) and other impacts on transportation, sporting activities (Doyle 2014; Mo et al. 2014), modifying the water levels in reservoirs (Jorg-Hess et al. 2015; Gurtz et al. 2003; Jonas et al. 2009), and modifying the water levels available for ecosystems (Semple 1918; Essery et al. 2009; Liston 1999). These suggest that accurate prediction of changes in snow precipitation is needed. As pointed out above, prediction of snow rate and amount are related to both in-cloud and ground-level microphysical, dynamical, and radiative processes. Therefore, more frequent and accurate measurements are needed in order to better understand and resolve these processes over the smaller scales (e.g., less than a few kilometers).

8. Challenges for understanding snow precipitation

The major challenges for improving snow precipitation predictions are related to gaps in our understanding of in-cloud processes (section 5) and surface snow measurements (section 3). Both issues affect modeling aspects of snow precipitation, including those

for both weather forecasting and climate modeling, and they are summarized below.

a. Measurement issues

The major issues with snow measurements are related to instrumental sensitivity and collection efficiency of snow crystals when environmental conditions change, for example, increasing wind speed and turbulence (Gultepe et al. 2016). Bogdanova et al. (2002) analyzed Arctic precipitation events and found that annual mean false precipitation detection makes up 30% or more of the total measured precipitation. In their work it is stated that blowing snow and blizzards significantly affect the quality of the in situ snow measurements (e.g., in coastal high-latitudinal regions, ice sheets, tundra, mountain desert, and steppe climatic zones), resulting in false precipitation detection. Unfortunately, light SN measurements cannot be measured accurately with weighing gauges such as Geonor or Pluvio (Gultepe et al. 2014a,b, 2016). Light snow PR is usually calculated by the measurements of OPWS (such as Vaisala PWD or Metek SWS) because of their lower threshold values for snow detection ($0.01\,\mathrm{mm\,h^{-1}}$) compared to the TPS and Geonor lower threshold of $0.5\,\mathrm{mm\,h^{-1}}$ without wind corrections (Rasmussen et al. 2012). Because of high winds and strong turbulence, error in SN measurements based on TPS can be large (Boudala et al. 2014). Above works suggest that measurement issues are still important over their evaluations in the cold climates and Arctic regions, and these are now summarized below.

1) Light snow measurements

The contribution of light snow precipitation amount, including ice crystals from clouds, ice fog crystals, and diamond dust particles, is important for hydrological assessment and weather applications (Gultepe et al. 2007, 2015, 2016; Girard and Blanchet 2001a,b; Yang et al. 2005; Huffman et al. 1995; Intrieri and Shupe 2004). Although heavy precipitation with large particles brings in large amounts of water over land and ocean surfaces, continuous light precipitation can play a much more important role in the growing season of plants, on aviation mission planning, and on the assessment of climate change. The LSN precipitation can also be responsible for discrepancies in precipitation retrievals between remote sensing platforms and in situ observations, and between model-based predictions and in situ–based observational analysis results. Gultepe et al. (2016) studied snow precipitation from the seven snow-measuring sensors (Fig. 6-13a) and found that large differences exist in PR$_{\mathrm{LSN}}$ measurements. Figure 6-13b
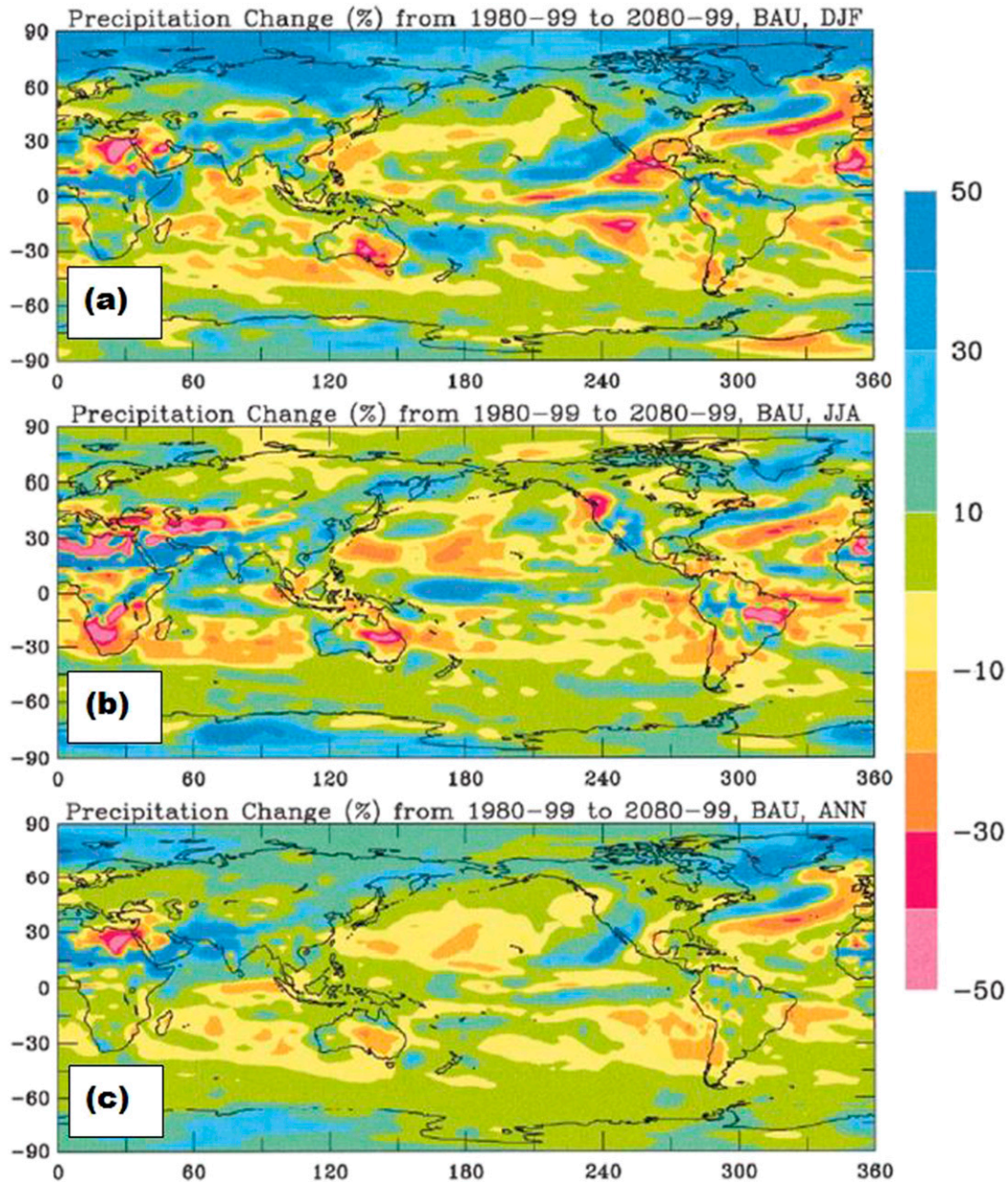
FIG. 6-12. Precipitation change (%) from the period 1980–99 to 2080–99 in the Consortium for the Application of Climate Impacts Assessments Business as Usual (ACACIA-BAU or BAU). BAU simulation for (a) DJF, (b) JJA, and (c) annual mean (adapted from Dai 2001).

shows that the GCIP sensor was much more sensitive to missing snow precipitation compared to others. These results suggested that light snow measurements need to be improved significantly.

2) CATCH EFFICIENCY AND BIAS FOR SNOW MEASUREMENTS

Catch efficiency, defined as the ratio of snow measurements to reference sensor measurements (e.g., DFIR), is obtained as a function of wind speed that is an important parameter to be considered for making accurate measurements of snow amount. Zhang et al. (2015) state that uncertainty in Geonor measurements can be about 44% when U_h is between 0.5 and 3.5 m s^{-1}, but when $U_h > 3.5$ m s^{-1} the Geonor could not measure any light snow. Bias corrections of snow measurements for weighing gauges can be related to wind-induced undercatch, wetting loss, and evaporation loss (Sevruk and
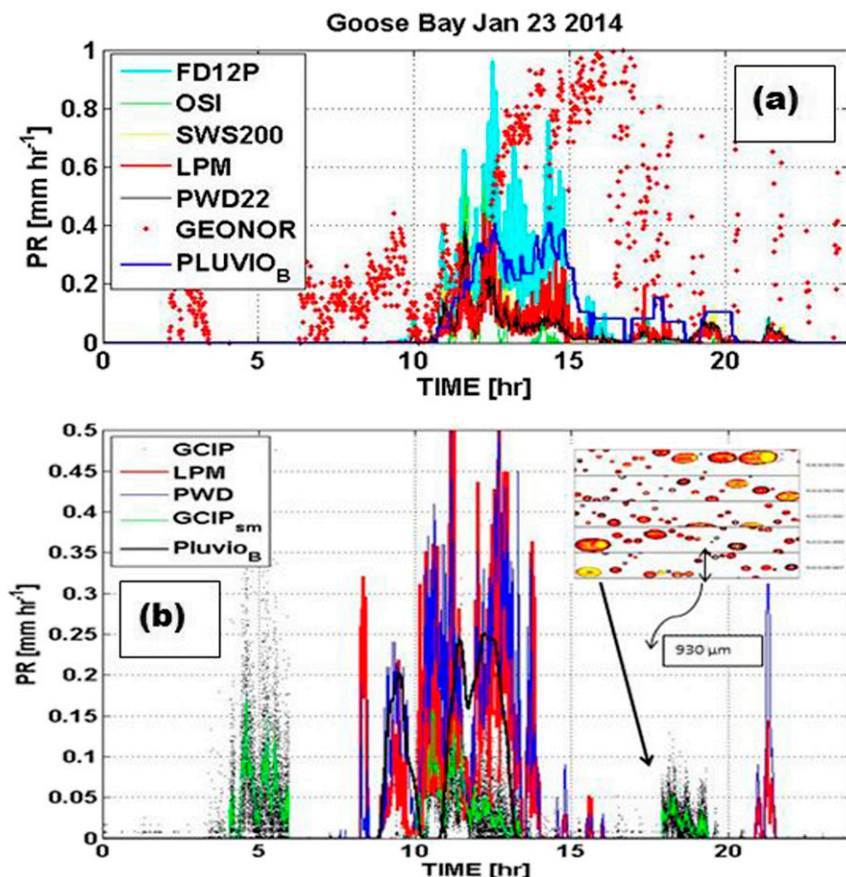
FIG. 6-13. The comparison of LSN precipitation rate from various instruments (see legend) on 23 Jan 2014 at $T \sim -18°C$ occurred over Goose Bay during the SAAWSO project. (a) Blowing snow effects seen after 1600 UTC are consistent with $U_h \sim 6\,m\,s^{-1}$. (b) Time series in UTC of GCIP-, LPM-, Pluvio-, and PWD-based LSN PR on 3 May 2014, Goose Bay. The black dots are for 1-Hz PR obtained from GCIP. The green solid line is for 60-s averages of GCIP PR to match with LPM- and PWD-based PR scales. The Pluvio-based PR is obtained using 60-min running averages. Freezing drizzle droplets occurred at 1830 UTC is seen in the inset panel.

Klemm 1989; Goodison 1981; Goodison et al. 1998). Light snow conditions can be affected by all these biases, but undercatch bias can be much stronger among these because of wind effects (Gultepe et al. 2016; Zhang et al. 2004). They found that during the cold seasons, bias with either wetting or evaporation can be about 15% and with undercatch, it can be more than 20%. This uncertainty can be removed from the observations significantly using protective oil products. In winter, evaporation and wetting losses together can be 0.10–0.20 mm day^{-1} (Aaltonen et al. 1993) and 0.15 mm day^{-1} (Sevruk 1982), respectively, for a total of about 0.5 mm day^{-1}. Figure 6-14a shows the results of Rasmussen et al. (2012) where a Geonor sensor with double-alter-shield catch efficiency is plotted versus wind speed. It shows that catch efficiency changes from about 0.25 to 1 as a function of wind speed. Figure 6-14b shows the differences

between Geonor sensors with various shields as a function time and wind speed. Geonor with double-alter-shield and DFIR-measured snow amounts were better than those of other setups, for example, the single-shield Geonor. Issues related to catch efficiency for solid particles are very important when their mass density is very small compared to wet particles, and it needs to be researched.

3) BLOWING SNOW

Blowing snow (BSN) conditions are related to strong winds and the age of snow on the ground. Increasing wind beyond a few meters per second can usually generate blowing snow conditions dependent on the age of snow and density of fresh snow. The BSN conditions in midlatitudes are considered when the wind speed >7 m s^{-1} (Trouvilliez et al. 2015), but
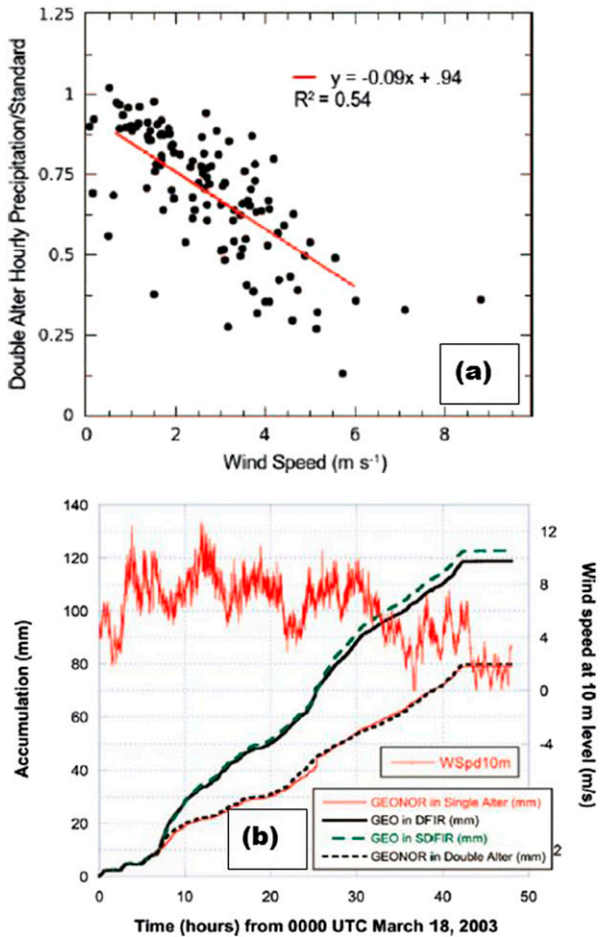
FIG. 6-14. (a) Hourly catch ratios of solid precipitation vs 1.5-m-height wind speeds. Double-alter-shielded Geonor measurements are normalized by the standard hourly precipitation amount. Best-fit equation (red line) is also shown on the plot with correlation coefficient. (b) Liquid equivalent accumulation in the Geonor with DFIR, small DFIR (SDFIR), and double-alter and single-alter shields for the 17–19 Mar blizzard. Wind speed is given by the red line and is indicated by the scale on the right (adapted from Rasmussen et al. 2012).

they can also occur often below this threshold at cold climates. If extreme wind conditions occur, SN measurements can be affected severely (Fig. 6-15a). This figure was taken for a BSN event that occurred during the winter of 2011 over Whistler Mountain in British Columbia, Canada. Some work considers that blowing snow conditions usually happen when $U_h > 7\,\mathrm{m\,s^{-1}}$ (Trouvilliez et al. 2015). But the impact of wind effects on SN measurements can be considered significant even when U_h is 1–$2\,\mathrm{m\,s^{-1}}$ at cold temperatures (Gultepe et al. 2016). Therefore, collection efficiency of snow particles at cold temperatures in northern latitudes should be evaluated differently compared to those of midlatitude conditions.

4) VARIABILITY IN SNOW DISTRIBUTION CONDITIONS

Variability in snow distribution over various conditions can play an important role for model validations and analyzing hydrological cycle over various geography conditions. Figure 6-15b shows an example of PR_{SN} and Vis, as well as horizontal wind measurements over the 500 m slope along the Whistler Mountain peak. This figure suggests that PR_{SN} can range between 1 and $3\,\mathrm{mm\,h^{-1}}$ along the 500-m slope (the three stations were about ~200 m apart) that significantly can affect validations of the forecast of snow predictions. Similar changes are also seen in Vis and wind observations. Therefore, numerical models should have high resolutions (<100 m) to capture the variability over mountainous and marine environments (Gultepe 2015). It should be noted that microphysical processes should be adjusted for representative scales because physical processes are scale dependent.

b. Snow prediction issues

Issues with snow precipitation prediction are related mainly to empirical relationships used among various microphysical parameters related to snow crystals mass, size, shape, density, fall velocities, ice crystal number concentration, and ice water content (Ferrier et al. 1996; Harrington et al. 2013a,b). This becomes more complicated when mixed-phase processes are considered. Also, microphysical algorithms dependent on model time and space scales, as well as autoconversion processes are major issues for snow prediction at the surface (McMillen and Steenburgh 2015a,b). In addition to prescribed microphysical schemes, newly developed particle growth-based MP schemes are being developed and these are provided in section 9.

1) AUTOCONVERSION PROCESSES

An important in-cloud processes affecting occurrence of PR_{SN} at the surface is related to how much in-cloud IWC or LWC will be converted to the precipitating particles. This complex process is usually related to the threshold values representing snow and ice crystal sizes. When snow crystal size exceeds a certain threshold, in-cloud ice particles fall out of their layer. This threshold can vary and the rate at which mass is transferred across this threshold is dependent on the dynamics of the system, environmental conditions (Heymsfield and Platt 1984), and the details of the aggregation process that converts small ice crystals to larger ones. (Lo and Passarelli 1982; Ferrier 1994). Figure 6-16 shows various autoconversion algorithms used in the model simulations (Liu et al. 2006). This figure suggests that variations in the methods developed for
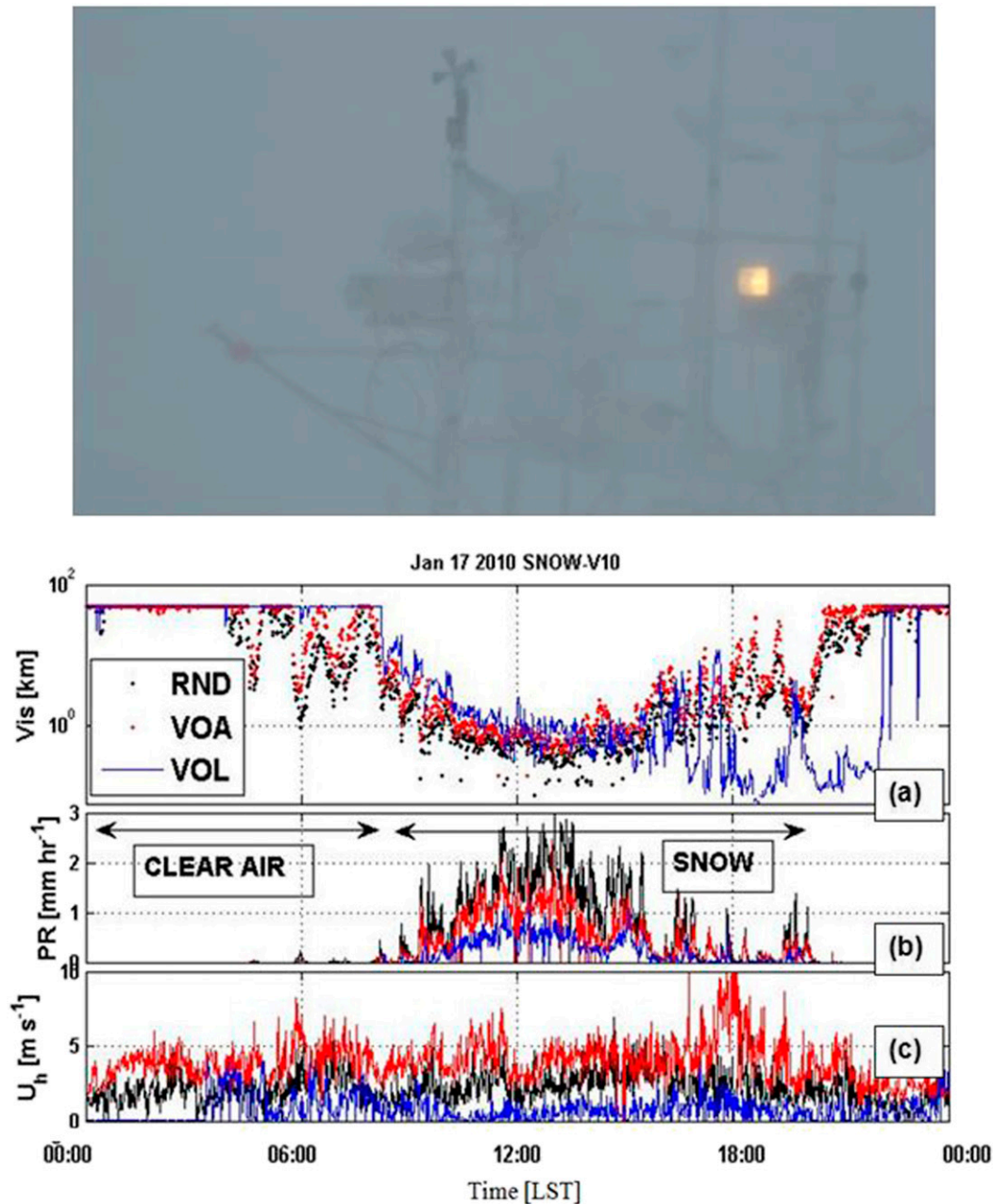
FIG. 6-15. (top) A blowing snow event happened during FRAM project at Roundhouse (RND) mountain site. Time series of (a) Vis, (b) PR from FD12P, and (c) U_h from 3D ultrasonic anemometer for RND, Whistler Mountain high-level (VOA), and Whistler Mountain midlevel (VOL) sites (black dots, red dots, and black solid line, respectively) show the vertical variability along a 500-m slope for 17 Jan 2010 (adapted from Gultepe et al. 2014a,b).

autoconversion processes play an important role for snow measurements and total water amount in cloud, and needs to be researched in greater detail.

2) ICE MULTIPLICATION

Cloud ice crystal particles can be enhanced by secondary ice processes that may occur by different pathways. The most common types are 1) the riming of the ice crystals (Heymsfield and Willis 2014; Lawson et al. 2015), 2) freely falling droplets while freezing at certain sizes resulting in splintering mechanism (Mossop and Wishart 1978), 3) collision fragmentation (Hobbs and Farber 1972; Jiusto and Weickmann 1973; Vardiman 1978), and 4) sublimation fragmentation [see
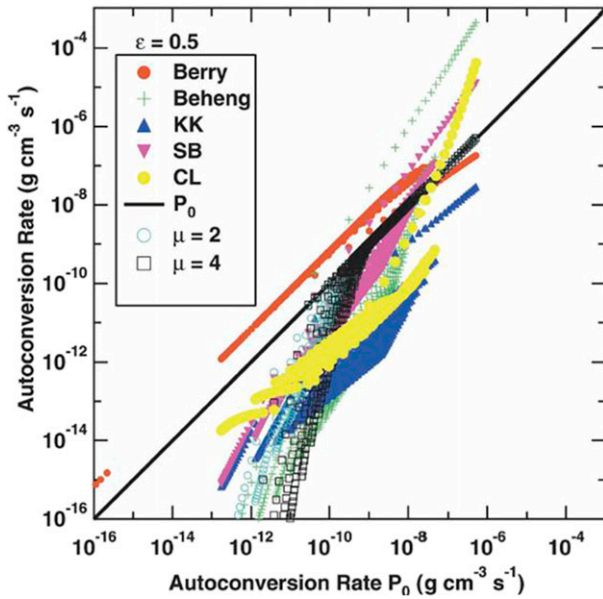
FIG. 6-16. Illustration of the new Sundqvist-type parameterization along with the previous autoconversion parameterizations. The two typical examples of the new Sundqvist-type parameterization shown here correspond to $\mu = 2$ and 4, respectively. Berry: Berry (1968); Beheng: Beheng (1994); KK: Khairoutdinov and Kogan (2000); SB: Seifert and Beheng (2001); CL: Chen and Liu (2004); P0: Liu–Daum rate function (Liu and Daum 2004) are also shown on the plot (adapted from Liu et al. 2006).

Field et al. (2017, chapter 7) for more details] Hallet and Mossop (1974) and Mossop (1976) suggested that the best conditions for the rime-splintering ice multiplication process are found for temperatures between $-3°$ and $-8°C$ (peak at about $-5°C$) within the saturated air with respect to water. Mossop et al. (1972; 1974) suggested that the N_i could exceed that of ice nuclei by a factor of 10^4 with cloud-top $T < -10°C$. This work indicates that a secondary ice multiplication process could play a major role in the evolution of snow precipitation. The ice enhancement factor as parameterized by Hobbs and Rangno (1990) uses a threshold value of droplet diameter where droplet number concentration N_d with a threshold diameter D_t should be greater than $3\,cm^{-3}$. Hobbs and Rangno (1985) also suggested that ice multiplication can be predicted when observed or predicted N_i is greater than that of Fletcher (1962). Increasing N_i due to ice multiplication processes can affect the phase of precipitation and in-cloud microphysical structure through microphysical process rates. Parameterizations for secondary ice crystal generations are not well constrained and are potentially an important issue for NWPs and climate models.

3) BULK VERSUS BIN MICROPHYSICS

Forecast models and climate models use various microphysical algorithms for in-cloud parameterizations and precipitation predictions. Because of the computational cost involved in the simulations, the choice of algorithm is related to the application of the model. The bulk microphysical algorithms are usually preferred for climate and weather applications because of their less expensive computational times. The bin microphysical algorithms represent cloud microphysical processes in more detail and they implement cloud processes more accurately; however, they are more computationally expensive compared to bulk schemes. Onishi and Takahashi (2012) showed that based on bin versus one- and two-moment schemes, precipitation at the surface can change significantly. Figure 6-17 shows their results for rain predictions at the surface. This figure suggests that various microphysical algorithms used in the models show significant differences in rainwater mixing ratio, and possibly can show much larger differences in the prediction of the snowfall as well (McMillen and Steenburgh 2015). Note that the two-moment schemes predict q_i and N_i prognostically; on the other hand, one-moment schemes use a parameterization for N_i prediction.

Global reanalysis are often applied for precipitation evaluation. The reanalysis use several fixed numerical weather prediction models and data assimilation schemes to produce gridded fields for PR over time periods suitable for climate research. Ballinger et al. (2013) conclude that caution must be exercised when using reanalysis data to study climate trends. Based on the reanalysis methods, climate change assessment is sensitive to the changes of the observing systems and processing methods (Bengtsson et al. 2004a,b; Sterl 2004). This is likely due to in-cloud processes such as the various microphysical algorithms mentioned above.

4) PRECIPITATION EFFECT ON FORECASTING OF VISIBILITY

For aviation and transportation application, Vis is usually a function of PR that shows increasing Vis with decreasing PR (Gultepe et al. 2015). The Vis–PR relationship for LSN (PR $< 0.5\,mm\,h^{-1}$) may not follow this indirect relationship. The NWS defines light snow when Vis $> 1\,km$. Rasmussen et al. (1999) used PR $< 1\,mm\,h^{-1}$ for LSN calculations. Under the LSN conditions, the NWS definition can be flawed because PR is not always indirectly related to Vis for PR $< 0.5\,mm\,h^{-1}$. In fact, there was a very light snow criterion in the past for the surface stations, but it was removed from reporting when there was no Vis restriction. A direct relationship between light snow PR and Vis completely contradicts the concept used by aviation applications. Under the LSN conditions, both Vis and PR can be very small because of suspended ice crystals, resulting in low Vis with small PR (Gultepe et al. 2016). This shows that accurate prediction of snow precipitation, if we ignore
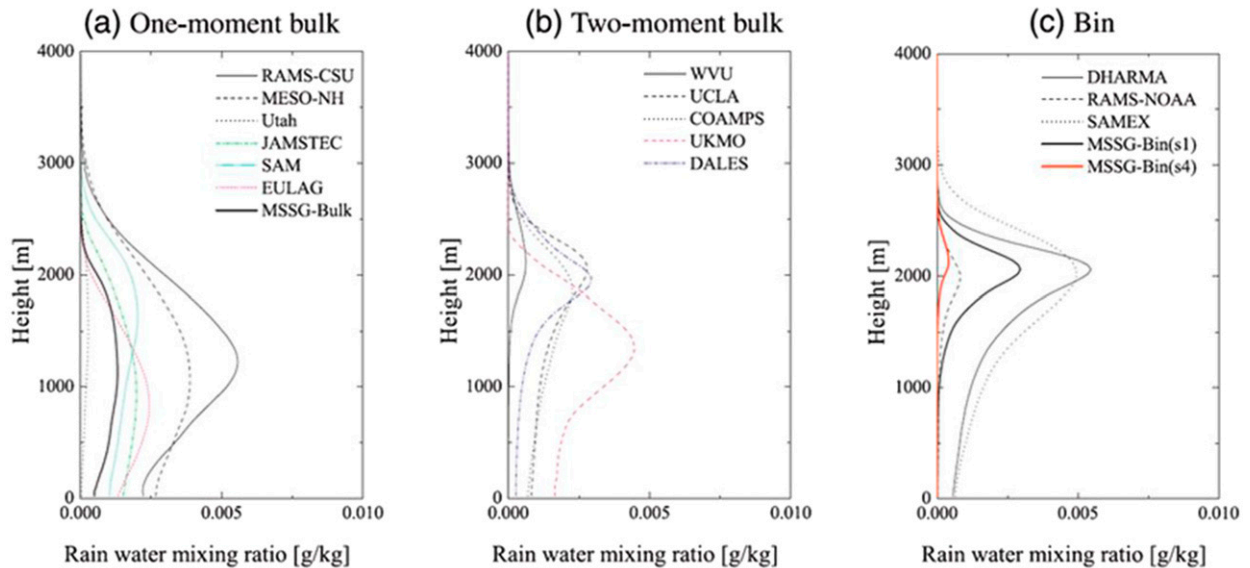
Fig. 6-17. Vertical profiles of rain mixing ratio based on various mesoscale models used for the same case study for (a) one-moment bulk models, (b) two-moment bulk models, and (c) bin models (adapted from Onishi and Takahashi 2012).

all other related parameters for improvement such as particle microphysics and optical properties, needs to be accurately performed; otherwise, relationships developed for Vis–PR will not hold.

9. Summary and recommendations for future research

Measurements and predictions of snow precipitation and in-cloud microphysical processes include important uncertainties, which have been described in this work. These uncertainties are also related to time- and space-scale variability, the chaotic nature of snow formation processes, and measurement errors, as well as processing the data with interpolation and areal sampling errors (Rudolf et al. 1994). These can also affect PR_{SN}, and precipitation trends and its energy equivalent values of PR to study global and local precipitation anomalies accurately. These issues can be significant over Arctic regions and continental climates where PR is less than a few hundreds of millimeters per year. It is possible that future precipitation studies, using observations from the Arctic observing satellites (Trishchenko et al. 2011) and the GPM satellite (Matsui et al. 2013), can improve the light snow observations but limitations of retrieval techniques related to the interaction of ice particles and radiation and ice cloud processes would still affect the quality of the LSN quantification.

Many of the microphysical processes for converting hydrometeors into graupel and hail are not well constrained. This is a topic that needs attention because of its strong contribution to surface precipitation and hazards occurring at the surface. For instance, both graupel and hail PSDs are usually derived from a very sparse set of measurements.

In the last few years there has been a shift in the way ice-phase hydrometeors are represented in microphysics schemes, diverting from the paradigm of using predefined categories with prescribed physical characteristics (e.g., bulk density) and converging on the prediction of the evolution of particle properties (e.g., Harrington et al. 2013a,b; Morrison and Milbrandt 2015). This has led to smoother evolution of ice crystals during growth and it avoids the artificial process of "conversion" between ice categories, which is an unphysical but inherently necessary feature of traditional, category-based microphysics schemes (bulk and bin) with arbitrary thresholds.

Microphysical schemes used in NWP and cloud models have been modified lately by new research (Morrison and Grabowski 2008) and developed into new ones (Harrington et al. 2013a,b; Morrison et al. 2015; Milbrandt and Morrison 2016). These works are promising to improve snow predictions as they describe a more physically realistic approach for snowfall evolution. In this approach, the autoconversion processes and hydrometeor classes are not used for snow evolution; meanwhile, hydrometeor types naturally evolve from the PSDs representing various particle phases. In-cloud processes such as aggregation, riming, ice multiplication, and mixing based on both observations and parameterizations should be studied in more

detail to better understand and develop microphysical schemes for numerical modeling applications. Improvements in measurements of snow precipitation can also be used for reducing uncertainties in the hydrological cycle and aviation mission planning. In the future, well designed projects will be needed for more detailed quantitative assessments of the SN effects on weather and climate issues over the Arctic and cold climates.

The small ice crystals, light snow, and drizzle precipitation rates over cold climates are important for weather and climate applications, and they cannot be measured by conventional instruments (e.g., weighing gauges) when $PR < 0.5 \, mm \, h^{-1}$ (Gultepe 2008; Gultepe et al. 2015). Also, correction of moderate and heavy snow measurements from weighing gauges because of wind and turbulence effects are needed to be improved for cold weather precipitation. Therefore, integration of observations based on various optical sensors is needed for better assessments of climate change and NWP simulations.

Overall, snow precipitation measurements are complex in nature because of various environmental effects on the sensors such as T, RH_w, and wind and turbulence. Snowfall prediction is related to how well the clouds are simulated with numerical weather prediction and climate models. This suggests a need for improvement of understanding in-cloud processes and accurate surface snow measurements that can lead to better prediction of cloud- and snow-related parameters.

REFERENCES

Aaltonen, A., E. Elomaa, A. Tuominen, and P. Valkovuori, 1993: Measurement of precipitation. *Proc. Symp. on Precipitation and Evaporation*, Bratislava, Slovakia, Slovak Hydrometeorological Institute and Swiss Federal Institute of Technology, 42–46.

American Meteorological Society, 2016a: Snow. Glossary of Meteorology. [Available at http://glossary.ametsoc.org/wiki/snow.]

——, 2016b: Graupel. Glossary of Meteorology. [Available at http://glossary.ametsoc.org/wiki/graupel.]

——, 2016c: Hail. Glossary of Meteorology. [Available at http://glossary.ametsoc.org/wiki/hail.]

Atlas, D., S. Y. Matrosov, A. J. Heymsfield, M.-D. Chou, and D. B. Wolff, 1995: Radar and radiation properties of ice clouds. *J. Appl. Meteor.*, **34**, 2329–2345, doi:10.1175/1520-0450(1995)034<2329:RARPOI>2.0.CO;2.

Ballinger, T. J., T. W. Schmidlin, and D. F. Steinhoff, 2013: The polar marine climate revisited. *J. Climate*, **26**, 3935–3952, doi:10.1175/JCLI-D-12-00660.1.

Barry, R. G., 1981: *Mountain Weather and Climate.* Methuen & Corp. Ltd., 313 pp.

Bechini, R., L. Baldini, and V. Chandrasekar, 2013: Polarimetric radar observations in the ice region of precipitating clouds at C-band and X-band radar frequencies. *J. Appl. Meteor. Climatol.*, **52**, 1147–1169, doi:10.1175/JAMC-D-12-055.1.

Beheng, K. D., 1994: A parameterization of warm cloud microphysical conversion processes. *Atmos. Res.*, **33**, 193–206, doi:10.1016/0169-8095(94)90020-5.

Bengtsson, L., S. Hagemann, and K. I. Hodges, 2004a: Can climate trends be calculated from reanalysis data? *J. Geophys. Res.*, **109**, D11111, doi:10.1029/2004JD004536.

——, K. I. Hodges, and S. Hagemann, 2004b: Sensitivity of the ERA40 reanalysis to the observing system: Determination of the global atmospheric circulation from reduced observations. *Tellus*, **56A**, 456–471, doi:10.1111/j.1600-0870.2004.00079.x.

Bergeron, T., 1935: On the physics of cloud and precipitation. *Proc. Fifth Assembly IUGG*, Lisbon, Portugal, International Union of Geodesy and Geophysics, 156–178.

Berry, E. X., 1968: Modification of the warm rain process. Preprints, *First National Conf. on Weather Modification*, Albany, NY, Amer. Meteor. Soc., 81–88.

Bogdanova, E. G., B. M. Ilyin, and I. V. Dragomilova, 2002: Application of a comprehensive bias-correction model to precipitation measured at Russian North Pole drifting stations. *J. Hydrometeor.*, **3**, 700–713, doi:10.1175/1525-7541(2002)003<0700:AOACBC>2.0.CO;2.

Boudala, F. S., R. Rasmussen, G. A. Isaac, and B. Scott, 2014: Performance of hot plate for measuring solid precipitation in complex terrain during the 2010 Vancouver Winter Olympics. *J. Atmos. Oceanic Technol.*, **31**, 437–446, doi:10.1175/JTECH-D-12-00247.1.

Braham, R. R., 1952: The water and energy budgets of the thunderstorm and their relation to thunderstorm development. *J. Meteor.*, **9**, 227–242, doi:10.1175/1520-0469(1952)009<0227:TWAEBO>2.0.CO;2.

Brandes, E. A., K. Ikeda, G. Zhang, M. Schönhuber, and R. M. Rasmussen, 2007: A statistical and physical description of hydrometeor distributions in Colorado snowstorms using a video disdrometer. *J. Appl. Meteor. Climatol.*, **46**, 634–650, doi:10.1175/JAM2489.1.

Browning, K. A., F. F. Hill, and C. W. Pardoe, 1974: Structure and mechanism of precipitation and the effect of orography in a wintertime sector. *Quart. J. Roy. Meteor. Soc.*, **100**, 309–330, doi:10.1002/qj.49710042505.

——, C. W. Pardoe, and F. F. Hill, 1975: The nature of orographic rain at wintertime cold fronts. *Quart. J. Roy. Meteor. Soc.*, **101**, 333–352, doi:10.1002/qj.49710142815.

Caylor, I. J., J. W. F. Goddard, S. E. Hopper, and A. J. Illingworth, 1990: Bright band errors in radar estimates of rainfall: Identification and correction using polarization diversity. *Weather Radar Networking*, C. G. Collier & M. Chapuis, Eds., COST Project 73, EUR 12414 EN-FR, Doc. EUCO-COST 73/52/90, 294–303.

Chen, J., and S. Liu, 2004: Physically based two-moment bulk water parameterizations for warm-cloud microphysics. *Quart. J. Roy. Meteor. Soc.*, **130**, 51–78, doi:10.1256/qj.03.41.

Choularton, T. W., and Coauthors, 2008: The influence of small aerosol particles on the properties of water and ice clouds. *Faraday Discuss.*, **137**, 205–222, doi:10.1039/B702722M.

Cimini, D., E. Westwater, and A. Gasiewski, 2010: Temperature and humidity profiling in the Arctic using ground-based millimeter-wave radiometry and 1DVAR. *IEEE Trans. Geosci. Remote Sens.*, **48**, 1381–1388, doi:10.1109/TGRS.2009.2030500.

——, and Coauthors, 2011: Thermodynamic atmospheric profiling during the 2010 Winter Olympics using ground-based microwave radiometry. *IEEE Trans. Geosci. Remote Sens.*, **49**, 4959–4969, doi:10.1109/TGRS.2011.2154337.

——, M. Nelson, J. Güldner, and R. Ware, 2015: Forecast indices from ground-based microwave radiometer for operational meteorology. *Atmos. Meas. Tech.*, **8**, 315–333, doi:10.5194/amt-8-315-2015.

Connolly, P. J., C. Emersic, and P. R. Field, 2012: A laboratory investigation into the aggregation efficiency of small ice crystals. *Atmos. Chem. Phys.*, **12**, 2055–2076, doi:10.5194/acp-12-2055-2012.

Cotton, R. J., and Coauthors, 2013: The effective density of small ice particles obtained from in situ aircraft observations of midlatitude cirrus. *Quart. J. Roy. Meteor. Soc.*, **139**, 1923–1934, doi:10.1002/qj.2058.

Dai, A., 2001: Global precipitation and thunderstorm frequencies. Part II: Diurnal variations. *J. Climate*, **14**, 1112–1128, doi:10.1175/1520-0442(2001)014<1112:GPATFP>2.0.CO;2.

Del Genio, A. D., M.-S. Yao, W. Kovari, and K. K.-W. Lo, 1996: A prognostic cloud water parameterization for global climate models. *J. Climate*, **9**, 270–304, doi:10.1175/1520-0442(1996)009<0270:APCWPF>2.0.CO;2.

Doyle, C., 2014: The impact of weather forecasts of various lead times on snowmaking decisions made for the 2010 Vancouver Olympic Winter Games. *Pure Appl. Geophys.*, **171**, 87–94, doi:10.1007/s00024-012-0609-y.

DMT Inc., 2004: Cloud Imaging Probe (CIP) manual. DMT Inc. DOC-0028 REV D, 43 pp.

Dubé, I., 2003: From mm to cm: Study of snow/liquid water ratios in Quebec. EWSO Rimouski Tech. Note, 127 pp.

Eito, H., and K. Aonashi, 2009: Verification of hydrometeor properties simulated by a cloud-resolving model using a passive microwave satellite and ground-based radar observations for a rainfall system associated with the baiu front. *J. Meteor. Soc. Japan*, **87A**, 425–446, doi:10.2151/jmsj.87A.425.

Elliott, R. D., and E. L. Hovind, 1964: The water balance of orographic clouds. *J. Appl. Meteor.*, **3**, 235–239, doi:10.1175/1520-0450(1964)003<0235:TWBOOC>2.0.CO;2.

Erfani, E., and D. L. Mitchell, 2016: Developing and bounding ice particle mass- and area-dimension expressions for use in atmospheric models and remote sensing. *Atmos. Chem. Phys.*, **16**, 4379–4400, doi:10.5194/acp-16-4379-2016.

Essery, R., and Coauthors, 2009: SNOWMIP2: An evaluation of forest snow process simulations. *Bull. Amer. Meteor. Soc.*, **90**, 1120–1135, doi:10.1175/2009BAMS2629.1.

Ferrier, B. S., 1994: A double-moment multiple-phase four-class bulk ice scheme. Part I: Description. *J. Atmos. Sci.*, **51**, 249–280, doi:10.1175/1520-0469(1994)051<0249:ADMMPF>2.0.CO;2.

——, W. K. Tao, and J. Simpson, 1995: A double-moment multiple-phase four-class bulk ice scheme. Part II: Simulations of convective storms in different large-scale environments and comparisons with other bulk parameterizations. *J. Atmos. Sci.*, **52**, 1001–1033, doi:10.1175/1520-0469(1995)052<1001:ADMMPF>2.0.CO;2.

——, J. Simpson, and W. K. Tao, 1996: Factors responsible for different precipitation efficiencies between midlatitude and tropical squall simulations. *Mon. Wea. Rev.*, **124**, 2100–2125, doi:10.1175/1520-0493(1996)124<2100:FRFPEI>2.0.CO;2.

Field, P. R., and A. J. Heymsfield, 2003: Aggregation and scaling of ice crystal size distributions. *J. Atmos. Sci.*, **60**, 544–560, doi:10.1175/1520-0469(2003)060<0544:AASOIC>2.0.CO;2.

——, and ——, 2015: Importance of snow to global precipitation. *Geophys. Res. Lett.*, **42**, 9512–9520, doi:10.1002/2015GL065497.

——, ——, and A. A. Bansemer, 2006: A test of ice self-collection kernels using aircraft data. *J. Atmos. Sci.*, **63**, 651–666, doi:10.1175/JAS3653.1.

——, ——, and ——, 2007: Snow size distribution parameterization for midlatitude and tropical ice clouds. *J. Atmos. Sci.*, **64**, 4346–4365, doi:10.1175/2007JAS2344.1.

——, and Coauthors, 2017: Secondary ice production: Current state of the science and recommendations for the future. *Ice Formation and Evolution in Clouds and Precipitation: Measurement and Modeling Challenges*, *Meteor. Monogr.*, No. 58, Amer. Meteor. Soc., doi:10.1175/AMSMONOGRAPHS-D-16-0014.1.

Fletcher, N. H., 1962: *The Physics of Rain Clouds.* Cambridge University Press, 386 pp.

Fujiyoshi, Y., T. Endoh, T. Yamada, K. Tsuboki, Y. Tachibana, and G. Wakahama, 1990: Determination of a *Z*–*R* relationship for snowfall using a radar and high sensitivity snow gauges. *J. Appl. Meteor.*, **29**, 147–152, doi:10.1175/1520-0450(1990)029<0147:DOARFS>2.0.CO;2.

Garrett, T. J., C. Fallgatter, K. Shkurko, and D. Howlett, 2012: Fall speed measurement and high-resolution multi-angle photography of hydrometeors in freefall. *Atmos. Meas. Tech.*, **5**, 2625–2633, doi:10.5194/amt-5-2625-2012.

Girard, E., and J. P. Blanchet, 2001a: Microphysical parameterization of Arctic diamond dust, ice fog, and thin stratus for climate models. *J. Atmos. Sci.*, **58**, 1181–1198, doi:10.1175/1520-0469(2001)058<1181:MPOADD>2.0.CO;2.

——, and ——, 2001b: Simulation of Arctic diamond dust, ice fog, and thin stratus using an explicit aerosol–cloud–radiation model. *J. Atmos. Sci.*, **58**, 1199–1221, doi:10.1175/1520-0469(2001)058<1199: SOADDI>2.0.CO;2.

Goodison, B. E., 1981: Compatibility of Canadian snowfall and snow cover data. *Water Resour. Res.*, **17**, 893–900, doi:10.1029/WR017i004p00893.

——, P. Y. T. Louie, and D. Yang, 1998: WMO solid precipitation measurement intercomparison. WMO Instruments and Observing Methods Final Rep. 67, WMO/TD-872, 212 pp.

Gruber, A., and V. Levizzani, 2008: Assessment of global precipitation products. World Climate Research Programme Rep. WCRP-128, WMO/TD 1430, 50 pp.

Güldner, J., and D. Spänkuch, 2001: Remote Sensing of the thermodynamic state of the atmospheric boundary layer by ground-based microwave radiometry. *J. Atmos. Oceanic Technol.*, **18**, 925–933, doi:10.1175/1520-0426(2001)018<0925: RSOTTS>2.0.CO;2.

Gultepe, I., 2008: Measurements of light rain, drizzle and heavy fog. *Precipitation: Advances in Measurement, Estimation and Prediction*, S. Michaelides, Ed., Springer-Verlag, 59–82.

——, 2015: Mountain weather: Observations and modeling. *Advances in Geophysics*, Vol. 56, Academic Press, 229–312, doi:10.1016/bs.agph.2015.01.001.

——, and Starr, D. O'C., 1995: Dynamical structure and turbulence in cirrus clouds: Aircraft observations during FIRE. *J. Atmos. Sci.*, **52**, 4659–4182, doi:10.1175/1520-0469(1995)052<4159: DSATIC>2.0.CO;2.

——, and B. Zhou, 2012: FTS (fog to snow) conversion process during the SNOW-V10 project. *Pure Appl. Geophys.*, **169**, 783–791, doi:10.1007/s00024-011-0349-4.

——, D. O'C. Starr, A. J. Heymsfield, T. Uttal, T. P. Ackerman, and D. L. Westphal, 1995: Dynamical characteristics of cirrus clouds from aircraft and radar observations in micro and meso-γ scales. *J. Atmos. Sci.*, **52**, 4060–4078, doi:10.1175/1520-0469(1995)052<4060:DCOCCF>2.0.CO;2.

——, G. Isaac, D. Hudak, R. Nissen, and W. Strapp, 2000: Dynamical and Microphysical characteristics of arctic clouds during BASE. *J. Climate*, **13**, 1225–1254, doi:10.1175/1520-0442(2000)013<1225:DAMCOA>2.0.CO;2.

——, and Coauthors, 2007: Fog research: A review of past achievements and future perspectives. *Pure Appl. Geophys.*, **164**, 1121–1159, doi:10.1007/s00024-007-0211-x.

——, and Coauthors, 2009: The Fog Remote Sensing and Modeling field project. *Bull. Amer. Meteor. Soc.*, **90**, 341–359, doi:10.1175/2008BAMS2354.1.

——, and Coauthors, 2014a: Ice fog in Arctic during FRAM–Ice Fog project: Aviation and nowcasting applications. *Bull. Amer. Meteor. Soc.*, **95**, 211–226, doi:10.1175/BAMS-D-11-00071.1.

——, G. A. Isaac, P. Joe, P. Kucera, J. Thériault, and T. Fisico, 2014b: Roundhouse (RND) mountain top research site: Measurements and uncertainties for winter alpine weather conditions. *Pure Appl. Geophys.*, **171**, 59–85, doi:10.1007/s00024-012-0582-5.

——, and Coauthors, 2015: A review on ice fog measurements and modeling. *Atmos. Res.*, **151**, 2–19, doi:10.1016/j.atmosres.2014.04.014.

——, R. Rabin, R. Ware, and M. Pavolonis, 2016: Light snow measurements over cold climatic regions. *Advances in Geophysics*, Vol. 57, Academic Press, 147–210, doi:10.1016/bs.agph.2016.09.001.

——, A. J. Heymsfield, M. Gallagher, L. Ickes, and D. Baumgardner, 2017: Ice fog: The current state of knowledge and future challenges.

Ice Formation and Evolution in Clouds and Precipitation: Measurement and Modeling Challenges, Meteor. Monogr., No. 58, Amer. Meteor. Soc., doi:10.1175/AMSMONOGRAPHS-D-16-0012.1.

Gurtz, J., M. Zappa, K. Jasper, H. Lang, M. Verbunt, A. Badoux, and T. Vitvar, 2003: A comparative study in modelling runoff and its components in two mountainous catchments. *Hydrol. Processes*, **17**, 297–311, doi:10.1002/hyp.1125.

Hallett, J., and S. C. Mossop, 1974: Production of secondary particles during the riming process. *Nature*, **249**, 26–58, doi:10.1038/249026a0.

Han, M., S. A. Braun, T. Matsui, and C. R. Williams, 2013: Evaluation of cloud microphysics schemes in simulations of a winter storm using radar and radiometer measurements. *J. Geophys. Res. Atmos.*, **118**, 1401–1419, doi:10.1002/jgrd.50115.

Harrington, J. Y., K. Sulia, and H. Morrison, 2013a: A method for adaptive habit prediction in bulk microphysical models. Part I: Theoretical development. *J. Atmos. Sci.*, **70**, 349–364, doi:10.1175/JAS-D-12-040.1.

——, ——, and ——, 2013b: A method for adaptive habit prediction in bulk microphysical models. Part II: Parcel model corroboration. *J. Atmos. Sci.*, **70**, 365–376, doi:10.1175/JAS-D-12-0152.1.

Harrison, D. L., S. J. Driscoll, and M. Kitchen, 2000: Improving precipitation estimates from weather radar using quality control and correction techniques. *Meteor. Appl.*, **7**, 135–144, doi:10.1017/S1350482700001468.

Heymsfield, A. J., 2003: Properties of tropical and midlatitude ice cloud particle ensembles. Part I: Median mass diameters and terminal velocities. *J. Atmos. Sci.*, **60**, 2573–2591, doi:10.1175/1520-0469(2003)060<2573:POTAMI>2.0.CO;2.

——, and C. M. R. Platt, 1984: A parameterization of the particle size spectrum of ice clouds in terms of the ambient temperature and the ice water content. *J. Atmos. Sci.*, **41**, 846–855, doi:10.1175/1520-0469(1984)041<0846:APOTPS>2.0.CO;2.

——, and C. D. Westbrook, 2010: Advances in the estimation of ice particle fall speeds using laboratory and field measurements. *J. Atmos. Sci.*, **67**, 2469–2482, doi:10.1175/2010JAS3379.1.

——, and P. Willis, 2014: Cloud conditions favoring secondary ice particle production in tropical maritime convection. *J. Atmos. Sci.*, **71**, 4500–4526, doi:10.1175/JAS-D-14-0093.1.

——, G. V. Zadelhoff, D. P. Donovan, F. Fabry, R. J. Hogan, and A. J. Illingworth, 2007: Refinements to ice particle mass dimensional and terminal velocity relationships for ice clouds. Part II: Evaluation and parameterizations of ensemble ice particle sedimentation velocities. *J. Atmos. Sci.*, **64**, 1068–1088, doi:10.1175/JAS3900.1.

——, P. R. Field, M. Bailey, D. Rogers, J. Stith, C. Twohy, Z. Wang, and S. Haimov, 2011: Ice in Clouds Experiment–Layer Clouds. Part I: Ice growth rates derived from lenticular wave cloud penetrations. *J. Atmos. Sci.*, **68**, 2628–2654, doi:10.1175/JAS-D-11-025.1.

Hobbs, P. V., 1975: The nature of winter clouds and precipitation in the Cascade Mountains and their modification by artificial seeding. Part I: Natural conditions. *J. Appl. Meteor.*, **14**, 783–804, doi:10.1175/1520-0450(1975)014<0783: TNOWCA>2.0.CO;2.

——, and R. J. Farber, 1972: Fragmentation of ice particles in clouds. *J. Rech. Atmos.*, **6**, 245–258.

——, and A. L. Rangno, 1985: Ice particle concentrations in clouds. *J. Atmos. Sci.*, **42**, 2523–2549, doi:10.1175/1520-0469(1985)042<2523: IPCIC>2.0.CO;2.

——, and ——, 1990: Rapid development of high ice particle concentrations in small polar maritime cumuliform clouds. *J. Atmos. Sci.*, **47**, 2710–2722, doi:10.1175/1520-0469(1990)047<2710:RDOHIP>2.0.CO;2.

Hogan, R. J., D. Bouniol, D. N. Ladd, E. J. O'Connor, and A. J. Illingworth, 2003: Absolute calibration of 94/95-GHz radars using rain. *J. Atmos. Oceanic Technol.*, **20**, 572–580, doi:10.1175/1520-0426(2003)20<572:ACOGRU>2.0.CO;2.

Hosler, C. L., and R. E. Hallgren, 1960: The aggregation of small ice crystals. *Discuss. Faraday Soc.*, **30**, 200–207, doi:10.1039/df9603000200.

Huang, G. J., V. N. Bringi, R. Cifelli, D. Hudak, and W. A. Petersen, 2010: A methodology to derive radar reflectivity–liquid equivalent snow rate relations using C-band radar and a 2D video disdrometer. *J. Atmos. Oceanic Technol.*, **27**, 637–650, doi:10.1175/2009JTECHA1284.1.

Huffman, G. J., R. F. Adler, B. Rudolf, U. Schneider, and P. R. Keehn, 1995: Global precipitation estimates based on a technique for combining satellite-based estimates, rain gauge analysis, and NWP model precipitation information. *J. Climate*, **8**, 1284–1295, doi:10.1175/1520-0442(1995)008<1284:GPEBOA>2.0.CO;2.

Iguchi, T., and Coauthors, 2012: Numerical analysis using WRF-SBM for the cloud microphysical structures in the C3VPfield campaign: Impacts of supercooled droplets and resultant riming on snow microphysics. *J. Geophys. Res.*, **117**, D23206, doi:10.1029/2012JD018101.

Intrieri, J. M., and M. D. Shupe, 2004: Characteristics and radiative effects of diamond dust over the western Arctic Ocean region. *J. Climate*, **17**, 2953–2960, doi:10.1175/1520-0442(2004)017<2953:CAREOD>2.0.CO;2.

Jaffrain, J., and A. Berne, 2011: Experimental quantification of the sampling uncertainty associated with measurements from PARSIVEL disdrometers. *J. Hydrometeor.*, **12**, 352–370, doi:10.1175/2010JHM1244.1.

Jiang, Q., and R. B. Smith, 2003: Gravity wave breaking in two-layer hydrostatic flow. *J. Atmos. Sci.*, **60**, 1159–1172, doi:10.1175/1520-0469(2003)060<1159:GWBITH>2.0.CO;2.

Jiusto, J. E., and H. K. Weickmann, 1973: Types of snowfall. *Bull. Amer. Meteor. Soc.*, **54**, 1148–1162, doi:10.1175/1520-0477(1973)054<1148:TOS>2.0.CO;2.

Jonas, T., C. Marty, and J. Magnusson, 2009: Estimating the snow water equivalent from snow depth measurements in the Swiss Alps. *J. Hydrol.*, **378**, 161–167, doi:10.1016/j.jhydrol.2009.09.021.

Jorg-Hess, S., N. Griessinger, and M. Zappa, 2015: Probabilistic forecasts of snow water equivalent and runoff in mountainous areas. *J. Hydrometeor.*, **16**, 2169–2186, doi:10.1175/JHM-D-14-0193.1.

Jung, Y., M. Xue, and G. Zhang, 2010: Simulations of polarimetric radar signatures of a supercell storm using a two-moment bulk microphysics scheme. *J. Appl. Meteor. Climatol.*, **49**, 146–163, doi:10.1175/2009JAMC2178.1.

Kajikawa, K., and A. J. Heymsfield, 1989: Aggregation of ice crystals in cirrus. *J. Atmos. Sci.*, **46**, 3108–3121, doi:10.1175/1520-0469(1989)046<3108:AOICIC>2.0.CO;2.

Kanji, Z. A., L. A. Ladino, H. Wex, Y. Boose, M. Burkert-Kohn, D. Cziczo, and M. Krämer, 2017: Overview of ice nucleating particles. *Ice Formation and Evolution in Clouds and Precipitation: Measurement and Modeling Challenges*, *Meteor. Monogr.*, No. 58, Amer. Meteor. Soc., doi:10.1175/AMSMONOGRAPHS-D-16-0006.1.

Kelly, R. D., and G. Vali, 1991: An experimental study of the production of ice crystals by a twin-turboprop aircraft. *J. Appl.*

Meteor., **30**, 217–226, doi:10.1175/1520-0450(1991)030<0217:AESOTP>2.0.CO;2.

Kennedy, P. C., and S. A. Rudledge, 2011: S-band dual-polarization radar observations of winter storms. *J. Appl. Meteor. Climatol.*, **50**, 844–858, doi:10.1175/2010JAMC2558.1.

Khairoutdinov, M., and Y. Kogan, 2000: A new cloud physics parameterization in a large-eddy simulation model of marine stratocumulus. *Mon. Wea. Rev.*, **128**, 229–243, doi:10.1175/1520-0493(2000)128<0229:ANCPPI>2.0.CO;2.

Knight, C. A., L. J. Miller, N. C. Knight, and D. Breed, 1982: *Precipitation Formation*. Vol. 2, *Hailstorms of the Central High Plains: Case Studies of the National Hail Research Experiment*, C. A. Knight and P. Squires, Eds., Colorado Associated University Press, 245 pp.

Knollenberg, R. G., 1969: Local cooling ice nucleation model. *J. Atmos. Sci.*, **26**, 125–129, doi:10.1175/1520-0469(1969)026<0125:TLCINM>2.0.CO;2.

——, 1972: Measurements of the growth of the ice budget in a persisting contrail. *J. Atmos. Sci.*, **29**, 1367–1374, doi:10.1175/1520-0469(1972)029<1367:MOTGOT>2.0.CO;2.

Knupp, K., R. Ware, D. Cimini, F. Vandenberghe, J. Vivekanandan, E. Westwater, and T. Coleman, 2009: Ground-based passive microwave profiling during dynamic weather conditions. *J. Atmos. Oceanic Technol.*, **26**, 1057–1073, doi:10.1175/2008JTECHA1150.1.

Knuth, S. L., G. J. Tripoli, J. E. Thom, and G. A. Weidner, 2010: The influence of blowing snow and precipitation on snow depth change across the Ross Ice Shelf and Ross Sea regions of Antarctica. *J. Appl. Meteor. Climatol.*, **49**, 1306–1321, doi:10.1175/2010JAMC2245.1.

Kuhn, T., and I. Gultepe, 2016: Ice fog and light snow measurements using a high-resolution camera system. *Pure Appl. Geophys.*, **173**, 3049–3064, doi:10.1007/s00024-016-1343-7.

Lang, S. E., W.-K. Tao, X. Zeng, and Y. Li, 2011: Reducing the biases in simulated radar reflectivities from a bulk microphysics scheme: Tropical convective systems. *J. Atmos. Sci.*, **68**, 2306–2320, doi:10.1175/JAS-D-10-05000.1.

Lawson, R. P., R. H. Cormack, and K. A. Weaver, 1993a: A new airborne precipitation spectrometer for atmospheric research. Preprints, *Eighth Symp. on Meteorological Observations and Instrumentation*, Anaheim, CA, Amer. Meteor. Soc., 30–35.

——, R. E. Stewart, J. W. Strapp, and G. A. Isaac, 1993b: Airborne measurements of the origin and growth of very large snowflakes. *Geophys. Res. Lett.*, **20**, 53–56, doi:10.1029/92GL02917.

——, ——, and L. J. Angus, 1998: Observations and numerical simulations of the origin and development of very large snowflakes. *J. Atmos. Sci.*, **55**, 3209–3229, doi:10.1175/1520-0469(1998)055<3209:OANSOT>2.0.CO;2.

——, S. Woods, and H. Morrison, 2015: The microphysics of ice and precipitation development in tropical cumulus clouds. *J. Atmos. Sci.*, **72**, 2429–2445, doi:10.1175/JAS-D-14-0274.1.

Leeper, R. D., J. Rennie, and M. A. Palecki, 2015: Observational perspectives from U.S. Climate Reference Network (USCRN) and Cooperative Observer Program (COOP): Temperature and precipitation comparison. *J. Atmos. Oceanic Technol.*, **32**, 703–721, doi:10.1175/JTECH-D-14-00172.1.

Li, L., G. M. Heymsfield, L. Tian, and P. E. Racette, 2005: Measurements of ocean surface backscattering using an airborne 94-GHz cloud radar—Implication for calibration of airborne and spaceborne W-band radars. *J. Atmos. Oceanic Technol.*, **22**, 1033–1045, doi:10.1175/JTECH1722.1.

Li, X., and Gao, S., 2011: Precipitation efficiency. *Precipitation Modeling and Quantitative Analysis*, Springer Atmospheric Sciences Series, Springer, 209–218.

——, C. H. Sui, and K. M. Lau, 2002: Precipitation efficiency in the tropical deep convective regime: A 2-D cloud resolving modeling study. *J. Meteor. Soc. Japan*, **80**, 205–212, doi:10.2151/jmsj.80.205.

——, W.-K. Tao, T. Matsui, C. Liu, and H. Masunaga, 2010: Improving a spectral bin microphysical scheme using TRMM satellite observations. *Quart. J. Roy. Meteor. Soc.*, **136**, 382–399.

Lin, Y. L., R. D. Farley, and H. D. Orville, 1983: Bulk parameterization of the snow field in a cloud model. *J. Climate Appl. Meteor.*, **22**, 1065–1092, doi:10.1175/1520-0450(1983)022<1065:BPOTSF>2.0.CO;2.

Liston, G. E., 1999: Interrelationships among snow distribution, snowmelt, and snow cover depletion: Implications for atmospheric, hydrologic, and ecologic modeling. *J. Appl. Meteor.*, **38**, 1474–1487, doi:10.1175/1520-0450(1999)038<1474:IASDSA>2.0.CO;2.

Liu, Y., and P. H. Daum, 2004: Parameterization of the autoconversion process. Part I: Analytical formulation of the Kessler type parameterizations. *J. Atmos. Sci.*, **61**, 1539–1548, doi:10.1175/1520-0469(2004)061<1539:POTAPI>2.0.CO;2.

——, ——, and R. McGraw, 2006: Parameterization of the autoconversion process. Part II: Generalization of Sundqvist-type parametrizations. *J. Atmos. Sci.*, **63**, 1103–1109, doi:10.1175/JAS3675.1.

Lloyd, G., and Coauthors, 2015: The origins of ice crystals measured in mixed-phase clouds at the high-alpine site Jungfraujoch. *Atmos. Chem. Phys.*, **15**, 12 953–12 969, doi:10.5194/acp-15-12953-2015.

Lo, K. K., and R. E. Passarelli Jr., 1982: The growth of snow in winter storms: An airborne observational study. *J. Atmos. Sci.*, **39**, 697–706, doi:10.1175/1520-0469(1982)039<0697:TGOSIW>2.0.CO;2.

Löhnert, U., S. Kneifel, A. Battaglia, M. Hagen, L. Hirsch, and S. Crewell, 2011: A multisensor approach toward a better understanding of snowfall microphysics: The TOSCA project. *Bull. Amer. Meteor. Soc.*, **92**, 613–628, doi:10.1175/2010BAMS2909.1.

MacDonald, J., and J. W. Pomeroy, 2007: Gauge undercatch of two common snowfall gauges in a prairie environment. *Proc. 64th Eastern Snow Conf.*, St. John's, NL, Canada, Eastern Snow Conference, 119–124.

Mailhot, J., J. A. Milbrandt, A. Giguere, R. McTaggart-Cown, A. Erfani, B. Denis, and A. Glazer, 2014: An experimental high-resolution forecast system during the Vancouver 2012 Winter Olympic and Paralympic Games. *Pure Appl. Geophys.*, **171**, 209–229, doi:10.1007/s00024-012-0520-6.

Matrosov, S. Y., 2015: Evaluations of the spheroidal particle model for describing cloud radar depolarization ratios of ice hydrometeors. *J. Atmos. Oceanic Technol.*, **32**, 865–879, doi:10.1175/JTECH-D-14-00115.1.

Matsui, T., X. Zeng, W. Tao, H. Masunaga, W. S. Olson, and S. Lang, 2009: Evaluation of long-term cloud-resolving model simulations using satellite radiance observations and multifrequency satellite simulators. *J. Atmos. Oceanic Technol.*, **26**, 1261–1274, doi:10.1175/2008JTECHA1168.1.

——, and Coauthors, 2013: GPM satellite simulator over ground validation sites. *Bull. Amer. Meteor. Soc.*, **94**, 1653–1660, doi:10.1175/BAMS-D-12-00160.1.

McFarquhar, G. M., and R. A. Black, 2004: Observations of particle size and phase in tropical cyclones: Implications for mesoscale modeling of microphysical processes. *J. Atmos. Sci.*, **61**, 422–439, doi:10.1175/1520-0469(2004)061<0422:OOPSAP>2.0.CO;2.

——, A. J. Heymsfield, J. Spinhirne, and B. Hart, 2000: Thin and subvisual tropopause tropical cirrus: Observations and radiative impacts. *J. Atmos. Sci.*, **57**, 1841–1853, doi:10.1175/1520-0469(2000)057<1841:TASTTC>2.0.CO;2.

——, M. S. Timlin, R. M. Rauber, B. F. Jewett, J. A. Grim, and D. P. Jorgensen, 2007: Vertical variability of cloud hydrometeors in the stratiform region of mesoscale convective systems and bow echoes. *Mon. Wea. Rev.*, **135**, 3405–3428, doi:10.1175/MWR3444.1.

McMillen, J. D. and W. J. Steenburgh, 2015a: Capabilities and limitations of convection-permitting WRF simulations of lake-effect systems over the Great Salt Lake. *Wea. Forecasting*, **30**, 1711–1731, doi:10.1175/WAF-D-15-0017.1.

——, and ——, 2015b: Impact of microphysics parameterizations on simulations of the 27 October 2010 Great Salt Lake–effect snowstorm. *Wea. Forecasting*, **30**, 136–152, doi:10.1175/WAF-D-14-00060.1.

Metcalfe, J. R., B. Routledge, and K. Devine, 1997: Rainfall measurement in Canada: Changing observational methods and archive adjustment procedures. *J. Climate*, **10**, 92–101, doi:10.1175/1520-0442(1997)010<0092:RMICCO>2.0.CO;2.

Milbrandt, J. A., and M. K. Yau, 2005: A multimoment bulk microphysics parameterization. Part II: A proposed three-moment closure and scheme description. *J. Atmos. Sci.*, **62**, 3065–3081, doi:10.1175/JAS3535.1.

——, and H. Morrison, 2016: Parameterization of cloud microphysics based on the prediction of bulk ice particle properties. Part III: Introduction of multiple free categories. *J. Atmos. Sci.*, **73**, 975–995, doi:10.1175/JAS-D-15-0204.1.

Mitchell, D. L., 1988: Evolution of snow-size spectra in cyclonic storms. Part I: Snow growth by vapor-deposition and aggregation. *J. Atmos. Sci.*, **45**, 3431–3452, doi:10.1175/1520-0469(1988)045<3431:EOSSSI>2.0.CO;2.

——, A. Huggins, and V. Grubisic, 2006: A new snow growth model with application to radar precipitation estimates. *Atmos. Res.*, **82**, 2–18, doi:10.1016/j.atmosres.2005.12.004.

Mo, R., and Coauthors, 2014: Mid-mountain clouds at Whistler during the Vancouver 2010 Winter Olympics and Paralympics. *Pure Appl. Geophys.*, **171**, 157–183, doi:10.1007/s00024-012-0540-2.

Morrison, H., and W. W. Grabowski, 2008: Modeling supersaturation and subgrid-scale mixing with two-moment bulk warm microphysics. *J. Atmos. Sci.*, **65**, 792–812, doi:10.1175/2007JAS2374.1.

——, and J. Milbrandt, 2011: Comparison of two-moment bulk microphysics schemes in idealized supercell thunderstorm simulations. *Mon. Wea. Rev.*, **139**, 1103–1130, doi:10.1175/2010MWR3433.1.

——, and ——, 2015: Parameterization of cloud microphysics based on the prediction of bulk ice particle properties. Part I: Scheme description and idealized tests. *J. Atmos. Sci.*, **72**, 287–311, doi:10.1175/JAS-D-14-0065.1.

——, J. A. Curry, and V. I. Khvorostyanov, 2005: A new double-moment microphysics parameterization for application in cloud and climate models. Part I: Description. *J. Atmos. Sci.*, **62**, 1665–1677, doi:10.1175/JAS3446.1.

——, J. A. Milbrandt, G. H. Bryan, K. Ikeda, S. A. Tessendorf, and G. Thompson, 2015: Parameterization of cloud microphysics based on the prediction of bulk ice particle properties. Part II: Case study comparisons with observations and

other schemes. *J. Atmos. Sci.*, **72**, 312–339, doi:10.1175/JAS-D-14-0066.1.

Mossop, S. C., 1976: Production of secondary ice particles during graupel by riming. *Quart. J. Roy. Meteor. Soc.*, **102**, 45–57, doi:10.1002/qj.49710243104.

——, 1978: The influence of the drop size distribution in the production of secondary ice particles during graupel growth. *Quart. J. Roy. Meteor. Soc.*, **104**, 323–330, doi:10.1002/qj.49710444007.

——, and E. R. Wishart, 1978: The mechanism of splintering during rime growth. *Geophys. Res. Lett.*, **5**, 1083–1085, doi:10.1029/GL005i012p01083.

——, A. Ono, and E. R. Wishart, 1970: Ice particles in maritime clouds near Tasmania. *Quart. J. Roy. Meteor. Soc.*, **96**, 487–508, doi:10.1002/qj.49709640910.

——, R. E. Cottis, and B. M. Bartlett, 1972: Ice crystal concentrations in cumulus and stratocumulus clouds. *Quart. J. Roy. Meteor. Soc.*, **98**, 105–123, doi:10.1002/qj.49709841509.

——, J. L. Brownscombe, and G. J. Collins, 1974: The production of secondary ice particles during riming. *Quart. J. Roy. Meteor. Soc.*, **100**, 427–436, doi:10.1002/qj.49710042514.

NWS, 1996: Table 2-14. Supplementary Observations, Part IV, Observing Handbook 7: Surface Observations, NOAA, 440 pp.

Onishi, R., and K. Takahashi, 2012: A warm bin-cold bulk hybrid cloud microphysical model. *J. Atmos. Sci.*, **69**, 1474–1497, doi:10.1175/JAS-D-11-0166.1.

Ovtchinnikov, M., and Y. L. Kogan, 2000: An investigation of ice production mechanisms in small cumuliform clouds using a 3D model with explicit microphysics. Part I: Model description. *J. Atmos. Sci.*, **57**, 2989–3003, doi:10.1175/1520-0469(2000)057<2989:AIOIPM>2.0.CO;2.

Passarelli, R. E., 1978: Theoretical and observational study of snow-size spectra and snowflake aggregation efficiencies. *J. Atmos. Sci.*, **35**, 882–889, doi:10.1175/1520-0469(1978)035<0882:TAOSOS>2.0.CO;2.

Pflaum, J. C., and H. R. Pruppacher, 1979: A wind tunnel investigation of the growth of graupel initiated from frozen drops. *J. Atmos. Sci.*, **36**, 680–689, doi:10.1175/1520-0469(1979)036<0680:AWTIOT>2.0.CO;2.

Phillips, V. T. J., M. Formenton, A. Bansemer, I. Kudzotsa, and B. Lienert, 2015: A parameterization of sticking efficiency for collisions of snow and graupel with ice crystals: Theory and comparison with observations. *J. Atmos. Sci.*, **72**, 4885–4902, doi:10.1175/JAS-D-14-0096.1.

Politovich, M., B. Stankov, and B. Martner, 1995: Determination of liquid water altitudes using combined remote sensors. *J. Appl. Meteor.*, **34**, 2060–2075, doi:10.1175/1520-0450(1995)034<2060:DOLWAU>2.0.CO;2.

Rabin, R., I. Gultepe, R. J. Kuligowski, and A. K. Heidinger, 2016: Satellite based snow precipitation prediction. *Pure Appl. Geophys.*, **173**, 3085–3102, doi:10.1007/s00024-015-1195-6.

Rasmussen, R., J. Vivekanandan, J. Cole, B. Myers, and C. Masters, 1999: The estimation of snowfall rate using visibility. *J. Appl. Meteor.*, **38**, 1542–1563, doi:10.1175/1520-0450(1999)038<1542:TEOSRU>2.0.CO;2.

——, M. Dixon, S. Vasiloff, F. Hage, S. Knight, J. Vivekanandan, and M. Xu, 2003: Snow nowcasting using a real-time correlation of radar reflectivity with snow gauge accumulation. *J. Appl. Meteor.*, **42**, 20–36, doi:10.1175/1520-0450(2003)042<0020:SNUART>2.0.CO;2.

——, and Coauthors, 2012: How well are we measuring snow: The NOAA/FAA/NCAR winter precipitation test bed. *Bull. Amer. Meteor. Soc.*, **93**, 811–829, doi:10.1175/BAMS-D-11-00052.1.

Rogers, D. C., and G. Vali, 1987: Ice crystal production by mountain surfaces. *J. Climate Appl. Meteor.*, **26**, 1152–1168, doi:10.1175/1520-0450(1987)026<1152:ICPBMS>2.0.CO;2.

Rosenfeld, D., and I. M. Lensky, 1998: Satellite-based insights into precipitation formation processes in continental and maritime convective clouds. *Bull. Amer. Meteor. Soc.*, **79**, 2457–2476, doi:10.1175/1520-0477(1998)079<2457:SBIIPF>2.0.CO;2.

Rudolf, B., and F. Rubel, 2005: Global precipitation. *Observed Global Climate*, M. Hantel, Ed., Landolt-Bornstein-Group V Geophysics Series, Vol. 6, Springer, 1–24.

——, H. Hauschild, W. Rüth, and U. Schneider, 1994: Terrestrial precipitation analysis: Operational method and required density of point measurements. *Global Precipitations and Climate Change*, M. Desbois and F. Désalmand, Eds., NATO ASI Series Vol. 26, Springer Verlag, 173–186.

Ryzhkov, A. V., and D. S. Zrnic, 2007: Depolarization in ice crystals and its effect on radar polarimetric measurements. *J. Atmos. Oceanic Technol.*, **24**, 1256–1267, doi:10.1175/JTECH2034.1.

——, M. Pinsky, A. Pokrovsky, and A. Khain, 2011: Polarimetric radar observation operator for a cloud model with spectral microphysics. *J. Appl. Meteor. Climatol.*, **50**, 873–894, doi:10.1175/2010JAMC2363.1.

Saleeby, S. M., W. R. Cotton, D. Lowenthal, and J. Messina, 2013: Aerosol impacts on the microphysical growth processes of orographic snowfall. *J. Appl. Meteor. Climatol.*, **52**, 834–852, doi:10.1175/JAMC-D-12-0193.1.

Sanchez, J., R. Posada, E. Garcia-Ortega, L. Lopez, and J. L. Marcos, 2013: A method to improve the accuracy of continuous measuring of vertical profiles of temperature and water vapor density by means of ground-based microwave radiometer. *Atmos. Res.*, **122**, 43–54, doi:10.1016/j.atmosres.2012.10.024.

Saunders, C. P. R., and N. M. A. Wahab, 1975: The influence of electric fields on the aggregation of ice crystals. *J. Meteor. Soc. Japan*, **53**, 121–126.

Sawyer, J. S., 1956: The physical and dynamical problems of orographic rain. *Weather*, **11**, 375–381, doi:10.1002/j.1477-8696.1956.tb00264.x.

Schmidt, R. B., 1991: The sublimation of snow intercepted by an artificial conifer. *Agric. For. Meteor.*, **54**, 1–27, doi:10.1016/0168-1923(91)90038-R.

Seifert, A., and K. D. Beheng, 2001: A double-moment parameterization for simulating autoconversion, accretion and self-collection. *Atmos. Res.*, **59-60**, 265–281, doi:10.1016/S0169-8095(01)00126-0.

Sekhon, R. S., and R. C. Srivastava, 1970: Snow size spectra and radar reflectivity. *J. Atmos. Sci.*, **27**, 299–307, doi:10.1175/1520-0469(1970)027<0299:SSSARR>2.0.CO;2.

Semple, E. C., 1918: The ancient Piedmont route of northern Mesopotamia. *Mon. Wea. Rev.*, **46**, 521, doi:10.1175/1520-0493(1918)46<521a:TAPRON>2.0.CO;2.

Serke, D., and Coauthors, 2014: Supercooled liquid water content profiling case studies with a new vibrating wire sonde compared to a ground-based microwave radiometer. *Atmos. Res.*, **149**, 77–87, doi:10.1016/j.atmosres.2014.05.026.

Sevruk, B., 1982: Method of correction for systematic error in point precipitation measurement for operational use. WMO Tech. Note WMO-589, 91 pp. [Available from WMO, Case Postale 2300, CH-1211, Geneva, Switzerland.]

——, and S. Klemm, 1989: Types of standard precipitation gauges. *Proc. Int. Workshop on Precipitation Measurements*, St. Moritz, Switzerland, WMO/IAHS/ETH, 227–236.

——, M. Ondrás, and B. Chvíla, 2009: The WMO precipitation measurement intercomparisons. *Atmos. Res.*, **92**, 376–380, doi:10.1016/j.atmosres.2009.01.016.

Shantz, N. C., I Gultepe, E. Andrews, A. Zelenyuk, M. E. Earle, A. M. Macdonald, P. S. K. Liu, and W. R. Leaitch, 2014: Optical, physical, and chemical properties of springtime aerosol over Barrow Alaska in 2008. *Int. J. Climatol.*, **34**, 3125–3138, doi:10.1002/joc.3898.

Smith, C. D., 2009: The relationship between snowfall catch efficiency and wind speed for the Geonor T-200B precipitation gauge utilizing various wind shield configurations. *Proc. 77th Western Snow Conf.*, Canmore, AB, Canada, Western Snow Conference, 115–121.

Smith, P. L., 1984: Equivalent radar reflectivity factors for snow and ice particles. *J. Climate Appl. Meteor.*, **23**, 1258–1260, doi:10.1175/1520-0450(1984)023<1258:ERRFFS>2.0.CO;2.

Solheim, F., J. Godwin, and R. Ware, 1998: Passive ground-based remote sensing of atmospheric temperature, water vapor, and cloud liquid water profiles by a frequency synthesized microwave radiometer. *Meteor. Z.*, **7**, 370–376.

Sterl, A., 2004: On the (in) homogeneity of reanalysis products. *J. Climate*, **17**, 3866–3873, doi:10.1175/1520-0442(2004)017<3866:OTIORP>2.0.CO;2.

Stoelinga, M. T., and T. T. Warner, 1999: Nonhydrostatic, mesobeta-scale model simulations of cloud ceiling and visibility for an east coast winter precipitation event. *J. Appl. Meteor.*, **38**, 385–404, doi:10.1175/1520-0450(1999)038<0385:NMSMSO>2.0.CO;2.

Sui, C. H., X. Li, M. J. Yang, and H. L. Huang, 2005: Estimation of oceanic precipitation efficiency in cloud models. *J. Atmos. Sci.*, **62**, 4358–4370, doi:10.1175/JAS3587.1.

——, ——, and ——, 2007: On the definition of precipitation efficiency. *J. Atmos. Sci.*, **64**, 4506–4513, doi:10.1175/2007JAS2332.1.

Sukovich, E. M., D. E. Kingsmill, and S. E. Yuter, 2009: Variability of graupel and snow observed in tropical oceanic convection by aircraft during TRMM KWAJEX. *J. Appl. Meteor. Climatol.*, **48**, 185–198, doi:10.1175/2008JAMC1940.1.

Sundqvist, H., E. Berge, and J. E. Kristjansonn, 1989: Condensation and cloud parameterization studies with a mesoscale numerical weather prediction model. *Mon. Wea. Rev.*, **117**, 1641–1657, doi:10.1175/1520-0493(1989)117<1641:CACPSW>2.0.CO;2.

Szyrmer, W., and I. Zwadzki, 2010: Snow studies. Part II: Average relationship between mass of snowflakes and their terminal fall velocity. *J. Atmos. Sci.*, **67**, 3319–3335, doi:10.1175/2010JAS3390.1.

Tao, W. K., D. Johnson, C. L. Shie, and J. Simpson, 2004: The atmospheric energy budget and large-scale precipitation efficiency of convective systems during TOGA COARE, GATE, SCSMEX, and ARM: Cloud-resolving model simulations. *J. Atmos. Sci.*, **61**, 2405–2423, doi:10.1175/1520-0469(2004)061<2405:TAEBAL>2.0.CO;2.

Tapiador, F. J., and Coauthors, 2012: Global precipitation measurement: Methods, datasets and applications. *Atmos. Res.*, **104–105**, 70–97, doi:10.1016/j.atmosres.2011.10.021.

Thies Clima, 2007: Laser precipitation monitor. Thies Clima Tech. Manual 5.4110.xx.x00 V2.2x STD, 58 pp.

Thompson, G., P. R. Field, R. M. Rasmussen, and W. D. Hall, 2008: Explicit forecasts of winter precipitation using an improved bulk microphysics scheme. Part II: Implementation of a new snow parameterization. *Mon. Wea. Rev.*, **136**, 5095–5115, doi:10.1175/2008MWR2387.1.

Tiedtke, M., 1993: Representation of clouds in large scale models. *Mon. Wea. Rev.*, **121**, 3040–3061, doi:10.1175/1520-0493(1993)121<3040:ROCILS>2.0.CO;2.

Tomita, H., 2008: New microphysical schemes with five and six categories by diagnostic generation of cloud ice. *J. Meteor. Soc. Japan*, **86A**, 121–142.

Trishchenko, A. P., L. Garand, and L. D. Trichtchenko, 2011: Three-apogee 16-h highly elliptical orbit as optimal choice for continuous meteorological imaging of polar regions. *J. Atmos. Oceanic Technol.*, **28**, 1407–1422, doi:10.1175/JTECH-D-11-00048.1.

Trouvilliez, A., F. N. Bouvet, H. Bellot, C. Genthon, and H. Gallée, 2015: Evaluation of the FlowCapt acoustic sensor for the aeolian transport of snow. *J. Atmos. Oceanic Technol.*, **32**, 1630–1641, doi:10.1175/JTECH-D-14-00104.1.

Turner, D., 2007: Improved ground-based liquid water path retrievals using a combined infrared and microwave approach. *J. Geophys. Res.*, **112**, D15204, doi:10.1029/2007JD008530.

Vardiman, L., 1978: The generation of secondary ice particles in clouds by crystal–crystal collision. *J. Atmos. Sci.*, **35**, 2168–2180, doi:10.1175/1520-0469(1978)035<2168:TGOSIP>2.0.CO;2.

Ware, R., and Coauthors, 2013: Thermodynamic and liquid profiling during the 2010 Winter Olympics. *Atmos. Res.*, **132–133**, 278–290, doi:10.1016/j.atmosres.2013.05.019.

Westwater, E., 1978: The accuracy of water vapor and cloud liquid determinations by dual-frequency ground-based microwave radiometry. *Radio Sci.*, **13**, 677–685, doi:10.1029/RS013i004p00677.

Williams, E. R., and S. Stanfill, 2002: The physical origin of the land–ocean contrast in lightning activity. *C. R. Phys.*, **3**, 1277–1292, doi:10.1016/S1631-0705(02)01407-X.

WMO, 2010: Guide to meteorological instruments and methods of observation. WMO Tech. Note 8, 17 pp.

WMO/CIMO, 1991: WMO solid precipitation measurement intercomparison. International Organizing Committee Fifth Session, Valdai, Russia, WMO Final Rep., 31 pp.

Wolfe, J. P., and J. R. Snider, 2012: A relationship between reflectivity and snow rate for a high-altitude S-band radar. *J. Appl. Meteor. Climatol.*, **51**, 1111–1128, doi:10.1175/JAMC-D-11-0112.1.

Xu, W., 2013: Precipitation and convective characteristics of summer deep convection over East Asia observed by TRMM. *Mon. Wea. Rev.*, **141**, 1577–1592, doi:10.1175/MWR-D-12-00177.1.

Yang, D., and Coauthors, 1999: Quantification of precipitation measurement discontinuity induced by wind shields on national gauges. *Water Resour. Res.*, **35**, 491–508, doi:10.1029/1998WR900042.

——, D. Kane, and Z. Zhang, 2005: Bias corrections of long-term (1973–2004) daily precipitation data over the northern regions. *Geophys. Res. Lett.*, **32**, L19501, doi:10.1029/2005GL024057.

Yuter, S. E., and R. A. Houze, 1995: Three-dimensional kinematic and microphysical evolution of Florida cumulonimbus. Part II: Frequency distributions of vertical velocity, reflectivity, and differential reflectivity. *Mon. Wea. Rev.*, **123**, 1941–1963, doi:10.1175/1520-0493(1995)123<1941:TDKAME>2.0.CO;2.

Zhang, D., Z. Wang, A. Heymsfield, J. Fan, and T. Luo, 2014: Ice concentration retrieval in stratiform mixed-phase clouds using

cloud radar reflectivity measurements and 1d ice growth model simulations. *J. Atmos. Sci.*, **71**, 3613–3635, doi:10.1175/JAS-D-13-0354.1.

Zhang, G., R. J. Doviak, D. S. Zrnić, R. Palmer, L. Lei, and Y. Al-Rashid, 2011a: Polarimetric phased-array radar for weather measurement: A planar or cylindrical configuration? *J. Atmos. Oceanic Technol.*, **28**, 63–73, doi:10.1175/2010JTECHA1470.1.

——, S. Luchs, A. Ryzhkov, M. Xue, L. Ryzhkova, and Q. Cao, 2011b: Winter Precipitation microphysics characterized by polarimetric radar and video disdrometer observations in central Oklahoma. *J. Appl. Meteor. Climatol.*, **50**, 1558–1570, doi:10.1175/2011JAMC2343.1.

Zhang, L., L. Zhao, C. Xie, G. Liu, L. Gao, Y. Xiao, J. Shi, and Y. Qiao, 2015: Intercomparison of solid precipitation derived from the weighting rain gauge and optical instruments in the interior Qinghai-Tibetan Plateau. *Adv. Meteor.*, 936724, doi:10.1155/2015/936724.

Zhang, Y., T. Ohata, D. Yang, and G. Davaa, 2004: Bias correction of daily precipitation measurements for Mongolia. *Hydrol. Processes*, **18**, 2991–3005, doi:10.1002/hyp.5745.

Zubler, E. M., U. Lohmann, D. Lüthi, C. Schär, and A. Muhlbaue, 2011: Statistical analysis of aerosol effects on simulated mixed-phase clouds and precipitation in the Alps. *J. Atmos. Sci.*, **68**, 1474–1492, doi:10.1175/2011JAS3632.1.